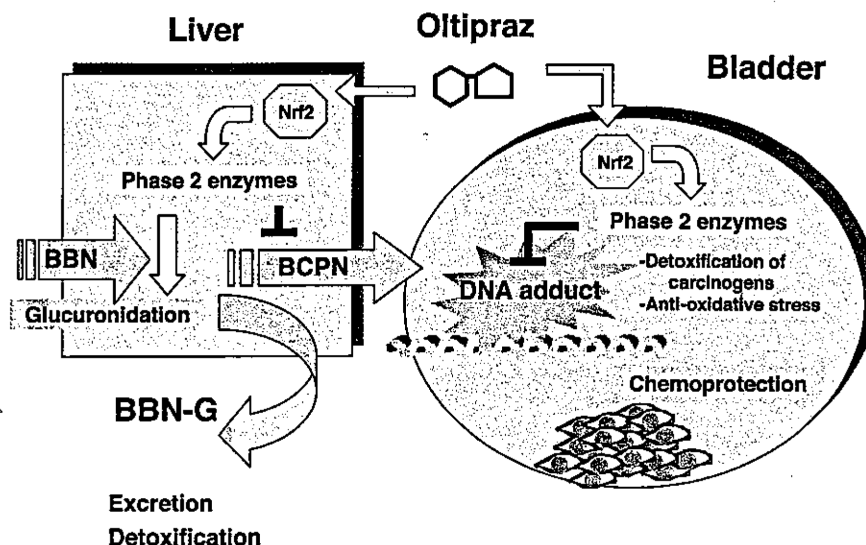

Fig. 6. Mechanism of chemoprotection by oltipraz against urinary bladder carcinogenesis. Oltipraz reduced BBN-induced carcinogenesis by suppressing the urinary excretion of BCPN by means of Nrf2-dependent induction of BBN glucuronidation in the liver. Moreover, oltipraz also works in the urinary bladder by inducing phase 2 enzymes and antioxidant proteins, such as HO-1, to suppress BBN-induced carcinogenesis. Furthermore, oltipraz counteracted the BBN-provoked urinary bladder-specific suppression of *UGT1A* gene expression in an Nrf2-dependent manner.

enzymes predisposes cells to neoplastic transformation. For example, Nelson *et al.* (48) reported that the loss of *GSTP1* expression in the prostate precedes neoplastic transformation. Expression of the *GSTP1* gene, which is the major GST isoform expressed in normal human prostate, is silenced in the majority of prostate tumors by the hypermethylation of CpG islands residing in the 5′ regulatory region. Conversely, overexpression of *GSTP1* in the prostate cell line LNCaP inhibited the cytotoxicity and DNA-adduct formation caused by a potential dietary carcinogen (49). Down-regulation of *UGT1A* gene expression also was found in an early stage of hepatocarcinogenesis (50).

In the case of urinary bladder cancer, it has been reported that carcinogenesis is associated with a decrease in or loss of *UGT1A* gene expression (13). Therefore, the finding that BBN acts to repress *UGT1A* gene expression in a urinary bladder-specific manner is intriguing. We found in this study that BBN significantly decreases *UGT1A* gene expression in a dose-dependent manner and that this decrease is observed as early as 1 day after administration of BBN (data not shown). This down-regulation of *UGT1A* leads to increased BBN or BCPN levels in urothelial cells, which may ultimately increase DNA alkylation. These observations also suggest the presence of bladder-specific regulation of *UGT1A* gene expression, which is sensitive to BBN. Because suppression also was observed in $Nrf2^{-/-}$ mice, the mechanism seems to be independent of Nrf2 regulation. In contrast, oltipraz counteracted the BBN-induced suppression in an Nrf2-dependent manner, suggesting that expression of *UGT1A* genes is under multiple regulatory influences. The Nrf2 regulatory pathway may compensate for the BBN-induced down-regulation of *UGT1A* gene expression in wild-type mice.

It was reported that *p53* gene knockout mice ($p53^{+/-}$ mice) are susceptible to BBN-induced urinary bladder carcinogenesis (43). The high susceptibility of $p53^{+/-}$ mice to BBN was associated with an increased cell proliferation without alteration of BCPN concentration in the urine. If we consider the high level of BCPN in the urine of $Nrf2^{-/-}$ mice, the mechanism that makes $Nrf2^{-/-}$ mice susceptible to BBN carcinogenesis must be different from that observed in $p53^{+/-}$ mice. Therefore, the use of a combination of oltipraz and other chemopreventive agents with distinct molecular targets would provide a strong synergistic efficacy. An attractive prospect also would be the discovery of more powerful chemical agents that are specifically delivered to the urinary bladder to induce the expression of phase 2 enzyme genes. Such strategies may be of importance in the protection against urinary bladder carcinogenesis.

ACKNOWLEDGMENTS

We thank Drs. Yukio Mori, Shigeru Taketani, John D. Hayes, Kimihiko Satoh, Shoji Fukushima, and Kit Tong for discussion and advice.

REFERENCES

1. Wai CY, Miller DS. Urinary bladder cancer. Clin Obstet Gynecol 2002;45:844–54.
2. Case RA, Hosker ME, McDonald DB, Pearson JT. Tumours of the urinary bladder in workmen engaged in the manufacture and use of certain dyestuff intermediates in the British chemical industry. Part I. The role of aniline, benzidine, α-naphthylamine, and β-naphthylamine. Br J Ind Med 1954;11:75–96.
3. Tricker AR, Mostafa MH, Spiegelhalder B, Preussmann R. Urinary excretion of nitrate, nitrite and N-nitroso compounds in schistosomiasis and bilharzia bladder cancer patients. Carcinogenesis 1989;10:547–52.
4. Mirvish SS. Role of N-nitroso compounds (NOC) and N-nitrosation in etiology of gastric, esophageal, nasopharyngeal and bladder cancer and contribution to cancer of known exposures to NOC. Cancer Lett 1995;93:17–48.
5. Druckrey H, Preussmann R, Ivankovic S, Schmahl D. Organotropic carcinogenic effects of 65 various N-nitroso- compounds on BD rats. Z Krebsforsch 1967;69:103–201.
6. IARC. N-Nitrosodi-n-butylamine. IARC Monogr Eval Carcinog Risk Chem Man 1978;17:51–75.
7. Okada M, Ishidate M. Metabolic fate of N-n-butyl-N-(4-hydroxybutyl)-nitrosamine and its analogues. Selective induction of urinary bladder tumours in the rat. Xenobiotica 1977;7:11–24.
8. Ito N, Hiasa Y, Tamai A, Okajima E, Kitamura H. Histogenesis of urinary bladder tumors induced by N-butyl-N-(4-hydroxybutyl)nitrosamine in rats. Gann 1969;60: 401–10.
9. Brockmoller J, Cascorbi I, Kerb R, Roots I. Combined analysis of inherited polymorphisms in arylamine N-acetyltransferase 2, glutathione S-transferases M1 and T1, microsomal epoxide hydrolase, and cytochrome P450 enzymes as modulators of bladder cancer risk. Cancer Res 1996;56:3915–25.
10. Johns LE, Houlston RS. N-acetyl transferase-2 and bladder cancer risk: a meta-analysis. Environ Mol Mutagen 2000;36:221–7.
11. Johns LE, Houlston RS. Glutathione S-transferase μ1 (GSTM1) status and bladder cancer risk: a meta-analysis. Mutagenesis 2000;15:399–404.
12. Park SJ, Zhao H, Spitz MR, Grossman HB, Wu X. An association between NQO1 genetic polymorphism and risk of bladder cancer. Mutat Res 2003;536:131–7.
13. Giuliani L, Gazzaniga P, Caporuscio F, Ciotti M, Frati L, Agliano AM. Can down-regulation of UDP-glucuronosyltransferases in the urinary bladder tissue impact the risk of chemical carcinogenesis? Int J Cancer 2001;91:141–3.
14. Hashimoto Y, Kitagawa HS. In vitro neoplastic transformation of epithelial cells of rat urinary bladder by nitrosamines. Nature 1974;252:497–99.
15. Airoldi L, Magagnotti C, Bonfanti M, Fanelli R. α-Oxidative metabolism of the bladder carcinogens N-nitrosobutyl(4-hydroxybutyl)amine and N-nitrosobutyl(3-carboxypropyl)-amine within the rat isolated bladder. Carcinogenesis 1990;11:1437–40.
16. Airoldi L, Magagnotti C, Bonfanti M, et al. Detection of O6-butyl- and O6-(4-hydroxy-butyl)guanine in urothelial and hepatic DNA of rats given the bladder carcinogen N-nitrosobutyl(4-hydroxybutyl)amine. Carcinogenesis 1994;15:2297–301.
17. Talalay P. Chemoprotection against cancer by induction of phase 2 enzymes. Biofactors 2000;12:5–11.
18. Talalay P, Dinkova-Kostova AT, Holtzclaw WD. Importance of phase 2 gene regulation in protection against electrophile and reactive oxygen toxicity and carcinogenesis. Adv Enzyme Regul 2003;43:121–34.
19. Benson AM, Batzinger RP, Ou SY, Bueding E, Cha YN, Talalay P. Elevation of hepatic glutathione S-transferase activities and protection against mutagenic metabolites of benzo(a)pyrene by dietary antioxidants. Cancer Res 1978;38:4486–95.

20. Ansher SS, Dolan P, Bueding E. Biochemical effects of dithiolethiones. Food Chem Toxicol 1986;24:405–15.
21. Zhang Y, Talalay P, Cho CG, Posner GH. A major inducer of anticarcinogenic protective enzymes from broccoli: isolation and elucidation of structure. Proc Natl Acad Sci USA 1992;89:2399–403.
22. Clapper ML. Chemopreventive activity of oltipraz. Pharmacol Ther 1998;78:17–27.
23. Kensler TW, Groopman JD, Sutter TR, Curphey TJ, Roebuck BD. Development of cancer chemopreventive agents: oltipraz as a paradigm. Chem Res Toxicol 1999;12:113–26.
24. Primiano T, Sutter TR, Kensler TW. Antioxidant-inducible genes. Adv Pharmacol 1997;38:293–328.
25. Friling RS, Bensimon S, Daniel V. Xenobiotic-inducible expression of murine glutathione S-transferase Ya subunit gene is controlled by an electrophile-responsive element. Proc Natl Acad Sci USA 1990;87:6258–62.
26. Rushmore TH, Morton MR, Pickett CB. The antioxidant responsive element. J Biol Chem 1991;266:11632–9.
27. Itoh K, Igarashi K, Hayashi N, Nishizawa M, Yamamoto M. Cloning and characterization of a novel erythroid cell-derived CNC family transcription factor heterodimerizing with the small maf family proteins. Mol Cell Biol 1995;15:4184–93.
28. Moi P, Chan K, Asunis I, Cao A, Kan YW. Isolation of NF-E2-related factor 2 (Nrf2), a NF-E2-like basic leucine zipper transcriptional activator that binds to the tandem NF-E2/AP1 repeat of the α-globin locus control region. Proc Natl Acad Sci USA 1994;91:9926–30.
29. Venugopal R, Jaiswal AK. Nrf1 and Nrf2 positively and c-Fos and Fra1 negatively regulate the human antioxidant response element-mediated expression of NAD(P)H: quinone oxidoreductase1 gene. Proc Natl Acad Sci USA 1996;93:14960–5.
30. Itoh K, Chiba T, Takahashi S, et al. An Nrf2/small Maf heterodimer mediates the induction of phase II detoxifying enzyme genes through antioxidant response elements. Biochem Biophys Res Commun 1997;236:313–22.
31. Chan K, Lu R, Chang JC, Kan YW. NRF2, a member of the NFE2 family of transcription factors, is not essential for murine erythropoiesis, growth, and development. Proc Natl Acad Sci USA 1996;93:13943–8.
32. Ishii T, Itoh K, Takahashi S, et al. Transcription factor Nrf2 coordinately regulates a group of oxidative stress-inducible genes in macrophages. J Biol Chem 2000;275:16023–9.
33. Ramos-Gomez M, Kwak MK, Dolan PM, et al. Sensitivity to carcinogenesis is increased and chemoprotective efficacy of enzyme inducers is lost in nrf2 transcription factor-deficient mice. Proc Natl Acad Sci USA 2001;98:3410–5.
34. Ramos-Gomez M, Dolan PM, Itoh K, Yamamoto M, Kensler TW. Interactive effects of nrf2 genotype and oltipraz on benzo[a]pyrene-DNA adducts and tumor yield in mice. Carcinogenesis 2003;24:461–7.
35. Fahey JW, Haristoy X, Dolan PM, et al. Sulforaphane inhibits extracellular, intracellular, and antibiotic-resistant strains of Helicobacter pylori and prevents benzo[a]pyrene-induced stomach tumors. Proc Natl Acad Sci USA 2002;99:7610–5.
36. Chan K, Han XD, Kan YW. An important function of Nrf2 in combating oxidative stress: detoxification of acetaminophen. Proc Natl Acad Sci USA 2001;98:4611–6.
37. Enomoto A, Itoh K, Nagayoshi E, et al. High sensitivity of Nrf2 knockout mice to acetaminophen hepatotoxicity associated with decreased expression of ARE-regulated drug metabolizing enzymes and antioxidant genes. Toxicol Sci 2001;59:169–77.
38. Chan K, Kan YW. Nrf2 is essential for protection against acute pulmonary injury in mice. Proc Natl Acad Sci USA 1999;96:12731–6.
39. Cho HY, Jedlicka AE, Reddy SP, et al. Role of NRF2 in protection against hyperoxic lung injury in mice. Am J Respir Cell Mol Biol 2002;26:175–82.
40. Aoki Y, Sato H, Nishimura N, Takahashi S, Itoh K, Yamamoto M. Accelerated DNA adduct formation in the lung of the Nrf2 knockout mouse exposed to diesel exhaust. Toxicol Appl Pharmacol 2001;173:154–60.
41. Oyasu R, Iwasaki T, Matsumoto M, Hirao Y, Tabuchi Y. Induction of tumors in heterotopic bladder by topical application of N-methyl-N-nitrosourea and N-butyl-N-(3-carboxypropyl)nitrosamine. Cancer Res 1978;38:3019–25.
42. Zhang YY, Ludwikowski B, Hurst R, Frey P. Expansion and long-term culture of differentiated normal rat urothelial cells in vitro. In Vitro Cell Dev Biol Anim 2001;37:419–29.
43. Ozaki K, Sukata T, Yamamoto S, et al. High susceptibility of p53(+/−) knockout mice in N-butyl-N-(4-hydroxybutyl)nitrosamine urinary bladder carcinogenesis and lack of frequent mutation in residual allele. Cancer Res 1998;58:3806–11.
44. Kumagai Y, Lin LY, Hiratsuka A, et al. Participation of cytochrome P450-2B and -2D isozymes in the demethylenation of methylenedioxymethamphetamine enantiomers by rats. Mol Pharmacol 1994;45:359–65.
45. Bonfanti M, Magagnotti C, Bonati M, Fanelli R, Airoldi L. Pharmacokinetic profile and metabolism of N-nitrosobutyl-(4-hydroxybutyl)amine in rats. Cancer Res 1988;48:3666–9.
46. Moon RC, Kelloff GJ, Detrisac CJ, Steele VE, Thomas CF, Sigman CC. Chemoprevention of OH-BBN-induced bladder cancer in mice by oltipraz, alone and in combination with 4-HPR and DFMO. Anticancer Res 1994;14:5–11.
47. Kang KW, Cho IJ, Lee CH, Kim SG. Essential role of phosphatidylinositol 3-kinase-dependent CCAAT/enhancer binding protein beta activation in the induction of glutathione S-transferase by oltipraz. J Natl Cancer Inst 2003;95:53–66.
48. Nelson CP, Kidd LC, Sauvageot J, et al. Protection against 2-hydroxyamino-1-methyl-6-phenylimidazo[4,5-b]pyridine cytotoxicity and DNA adduct formation in human prostate by glutathione S-transferase P1. Cancer Res 2001;61:103–9.
49. Nelson WG, De Marzo AM, Deweese TL, et al. Preneoplastic prostate lesions: an opportunity for prostate cancer prevention. Ann NY Acad Sci 2001;952:135–44.
50. Strassburg CP, Manns MP, Tukey RH. Differential down-regulation of the UDP-glucuronosyltransferase 1A locus is an early event in human liver and biliary cancer. Cancer Res 1997;57:2979–85.

Genetic ablation of Nrf2 enhances susceptibility to cigarette smoke–induced emphysema in mice

Tirumalai Rangasamy,[1] Chung Y. Cho,[2] Rajesh K. Thimmulappa,[1] Lijie Zhen,[2] Sorachai S. Srisuma,[1] Thomas W. Kensler,[1,3] Masayuki Yamamoto,[4] Irina Petrache,[5] Rubin M. Tuder,[2,5] and Shyam Biswal[1,3]

[1]Department of Environmental Health Sciences, Bloomberg School of Public Health, [2]Department of Pathology, School of Medicine, [3]Department of Oncology, Sidney Kimmel Comprehensive Cancer Center, Johns Hopkins University, Baltimore, Maryland, USA. [4]Center for Tsukuba Advanced Research Alliance and Institute of Basic Medical Sciences, University of Tsukuba, Tsukuba, Japan. [5]Division of Pulmonary and Critical Care Medicine, Department of Medicine, School of Medicine, Johns Hopkins University, Baltimore, Maryland, USA.

Although inflammation and protease/antiprotease imbalance have been postulated to be critical in cigarette smoke–induced (CS-induced) emphysema, oxidative stress has been suspected to play an important role in chronic obstructive pulmonary diseases. Susceptibility of the lung to oxidative injury, such as that originating from inhalation of CS, depends largely on its upregulation of antioxidant systems. Nuclear factor, erythroid-derived 2, like 2 (Nrf2) is a redox-sensitive basic leucine zipper protein transcription factor that is involved in the regulation of many detoxification and antioxidant genes. Disruption of the *Nrf2* gene in mice led to earlier-onset and more extensive CS-induced emphysema than was found in wild-type littermates. Emphysema in *Nrf2*-deficient mice exposed to CS for 6 months was associated with more pronounced bronchoalveolar inflammation; with enhanced alveolar expression of 8-oxo-7,8-dihydro-2′-deoxyguanosine, a marker of oxidative stress; and with an increased number of apoptotic alveolar septal cells — predominantly endothelial and type II epithelial cells — as compared with wild-type mice. Microarray analysis identified the expression of nearly 50 Nrf2-dependent antioxidant and cytoprotective genes in the lung that may work in concert to counteract CS-induced oxidative stress and inflammation. The responsiveness of the Nrf2 pathway may act as a major determinant of susceptibility to tobacco smoke–induced emphysema by upregulating antioxidant defenses and decreasing lung inflammation and alveolar cell apoptosis.

Introduction

Pulmonary emphysema is a major manifestation of chronic obstructive pulmonary disease (COPD), which affects more than 16 million Americans and is the fourth highest cause of death in United States (1). COPD is the only disease among the top 10 causes of death with rising incidence in the United States, and it is predicted to reach worldwide epidemic proportions (2). Cigarette smoking accounts for most of this debilitating disease, but other environmental risk factors include air pollution and chronic occupational exposure to various dusts (3).

Permanent destruction of peripheral air spaces distal to terminal bronchioles is the hallmark of emphysema (4). Emphysema is also characterized by accumulation of inflammatory cells such as macrophages and neutrophils (1) in bronchioles and alveolar structures. In humans, a deficiency in antiproteinase inhibitors produced by inflammatory cells, such as α1-antitrypsin, has been shown to contribute to a protease/antiprotease imbalance, thereby favoring destruction of alveolar extracellular matrix in cigarette smoke–induced (CS-induced) emphysema (5, 6). MMPs play a central role in experimental emphysema, as documented by the resistance of macrophage metalloelastase knockout mice against emphysema caused by chronic inhalation of CS (7). Moreover, pulmonary overexpression of interleukin-13 in transgenic mice results in MMP- and cathepsin-dependent emphysema (8). There is recent evidence that apoptosis of alveolar septal cells also contributes to human emphysema and is required for experimental emphysema caused by inhibition of the vascular endothelial growth factor receptor (4).

Markers of oxidative stress (e.g., hydrogen peroxide and the end products of lipid peroxidation such as ethane, pentane, and 8-isoprostane) are elevated in the breath and serum of patients with COPD (9). Oxidative stress enhances inflammation, inactivates critical antiproteinase inhibitors such as α1-antitrypsin (10), and enhances apoptosis of alveolar cells (4). Inflammatory mediators such as interleukin-8 and tumor necrosis factor-α, which are increased in bronchoalveolar samples obtained from patients with COPD (10, 11), are regulated by proinflammatory redox-sensitive transcription factors, including nuclear factor-κB and activator protein-1. Numerous studies have demonstrated that the susceptibility of the lung to oxidative injury depends largely on the upregulation of protective antioxidant systems (10). Although oxidative stress, which originates from CS and infiltrating inflammatory cells, is suspected to be involved in the etiopathogenesis of

Nonstandard abbreviations used: ARE, antioxidant response element; BAL, bronchoalveolar lavage; COPD, chronic obstructive pulmonary disease; CS, cigarette smoke; EMSA, electrophoretic mobility shift assay; G6PDH, glucose-6-phosphate dehydrogenase; γ-GCS, γ-glutamyl cysteine synthase; GPx, glutathione peroxidase; GSR, glutathione reductase; GST, glutathione S-transferase; HO-1, heme oxygenase-1; NQO1, NADPH: quinone oxidoreductase-1; Nrf2, nuclear factor, erythroid-derived 2, like 2; OCT1, octamer transcription factor 1; 8-oxo-dG, 8-oxo-7,8-dihydro-2′-deoxyguanosine; Prx-1, peroxiredoxin-1; SpC, surfactant protein C; TrxR, thioredoxin reductase; TSS, transcription start site; UGT, UDP-glucuronosyl transferase.

Conflict of interest: The authors have declared that no conflict of interest exists.

Citation for this article: *J. Clin. Invest.* **114**:1248–1259 (2004). doi:10.1172/JCI200421146.

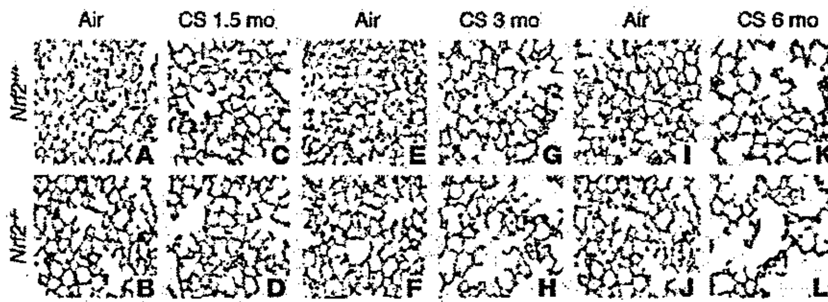

Figure 1
Increased susceptibility of *Nrf2*$^{-/-}$ mice to CS-induced emphysema. Shown are H&E-stained lung sections from *Nrf2*$^{+/+}$ and *Nrf2*$^{-/-}$ mice exposed to air alone (**A** and **B**, **E** and **F**, and **I** and **J**) and to CS (**C** and **D**, **G** and **H**, and **K** and **L**) at the indicated times. Sections from the air-exposed *Nrf2*$^{+/+}$ and *Nrf2*$^{-/-}$ mice show normal alveolar structure (n = 5 per group). Lung sections from the CS-treated (6 months) *Nrf2*$^{-/-}$ mice show increased air space enlargement when compared with the lung sections from the CS-treated *Nrf2*$^{+/+}$ mice. Original magnification, ×20.

the disease (10), there is no conclusive experimental evidence that supports a central role for oxidative stress in pathogenesis of CS-induced emphysema. Critical host factors that protect the lungs against oxidative stress may either directly determine susceptibility to alveolar tissue destruction in emphysema or act as modifiers of risk by affecting the intensity of inflammation associated with chronic CS inhalation.

Linkage analysis of hyperoxia-resistant and -sensitive mouse strains have identified *nuclear factor, erythroid-derived 2, like 2* (*Nrf2*) as a candidate gene for resistance to hyperoxic injury (12). *Nrf2* encodes a basic leucine zipper protein (bZIP) transcription factor which, upon activation in response to oxidative or electrophilic stress, detaches from its cytosolic inhibitor, Keap1, translocates to the nucleus, and binds to the antioxidant response element (ARE) in the promoter of target genes, leading to their transcriptional induction (13). Though little is known about Nrf2-regulated genes in the lungs, the recognized members of this group include several critical antioxidant genes, such as heme oxygenase-1 (HO-1), γ-glutamyl cysteine synthase (γ-GCS), and several members of the glutathione S-transferase (GST) family (13).

We have postulated that Nrf2 is a critical transcription factor that determines susceptibility to lung inflammation, oxidative stress, and alveolar cell apoptosis caused by chronic exposure to CS. In the present study, we demonstrate that disruption of the *Nrf2* gene led to earlier-onset and more extensive CS-induced emphysema in mice. Thus, responsiveness of the Nrf2 pathway in lung cells plays a critical role in attenuating the development of CS-induced emphysema.

Results

Histological and lung morphometric studies. Lungs from air-exposed *Nrf2*-disrupted (*Nrf2*$^{-/-}$) and wild-type (*Nrf2*$^{+/+}$) mice showed normal alveolar structure (Figure 1). Since the alveolar diameter of air-exposed *Nrf2*$^{-/-}$ mice was slightly smaller than that of air-exposed wild-type mice (Table 1), we undertook detailed lung morphometric measurements, as well as light microscopic and ultrastructural studies, to ensure that *Nrf2*$^{-/-}$ lung does not have delayed development or compromised structural integrity when maintained in normal room air. There were no significant differences in alveolar diameter and mean linear intercept between *Nrf2*$^{+/+}$ and *Nrf2*$^{-/-}$ lungs at 3 days, 10 days, 2 months, or 6 months of age (Supplemental Figure 1, A–C; supplemental material available at http://www.jci.org/cgi/content/full/114/1248/9/DC1). Histochemical staining for reticulin and elastin showed similar alveolar architecture in the wild-type and knockout lungs, with progressive attenuation of alveolar septa occurring between day 10 and 2 months of age in both genetic backgrounds (Supplemental Figure 1A). At 2 months of age, there was no significant difference in the total lung capacity (Supplemental Methods) between the air-exposed *Nrf2*$^{+/+}$ (1.19 ± 0.16 ml; average weight of mice, 23 ± 1.4 g) and *Nrf2*$^{-/-}$ mice (1.12 ± 0.19 ml; average weight of mice, 23 ± 1.2 g), and the proliferation rate was similar in *Nrf2*$^{+/+}$ and *Nrf2*$^{-/-}$ lungs (Supplemental Figure 1D). Finally, *Nrf2*$^{+/+}$ and *Nrf2*$^{-/-}$ lungs had similar ultrastructural alveolar organization, with alveolar-capillary membranes lined by type I epithelial cells, and both had normal alveolar type II cell populations (Supplemental Figure 2, A and B). Histological examination of the lung sections did not reveal any tumors in air- or CS-exposed mice. Furthermore, H&E-stained lung sections did not show any significant inflammation in the lungs of air-exposed *Nrf2*$^{+/+}$ or *Nrf2*$^{-/-}$ mice (Figure 1 and Supplemental Figure 1A).

To determine the role of Nrf2 in susceptibility to CS-induced emphysema, *Nrf2*-disrupted and wild-type *Nrf2* (ICR strain) mice were exposed to CS for 1.5 to 6 months, and CS-induced lung damage was assessed by computer-assisted morphometry. There was a dramatic increase in alveolar destruction in the lungs of *Nrf2*-disrupted mice when compared to wild-type ICR mice after 6 months of exposure to CS. Both the alveolar diameter (increased by 33.1% in *Nrf2*$^{-/-}$ vs. 8.5% in *Nrf2*$^{+/+}$ mice) and mean linear intercept (increased by 26.1% in *Nrf2*$^{-/-}$ vs. 8.3% in *Nrf2*$^{+/+}$ mice) were significantly higher in CS-exposed *Nrf2*-disrupted mice (Table 1 and Figure 1). Alveolar enlargement was detected in the lungs of *Nrf2*$^{-/-}$ mice as early as 3 months after exposure to CS began (Table 1 and Figure 1), suggesting an earlier onset of emphysema in *Nrf2*-disrupted mice. Long-term (6 months) exposure of *Nrf2*$^{+/+}$ mice to CS resulted in an increase of less than 10% in the mean linear intercept and alveolar

Table 1
Effect of chronic exposure to CS on lung morphometry

Groups	Time of exposure (mo)	Alveolar diameter (μm) Air	CS	% Increase	Mean linear intercept (μm) Air	CS	% Increase
Nrf2$^{+/+}$	1.5	37.2 ± 1.3	39.1 ± 1.5	5.1	51.9 ± 2.3	52.3 ± 1.8	1.9
	3	37.5 ± 1.6	40.5 ± 1.4	7.9	51.8 ± 2.7	53.6 ± 1.6	3.3
	6	38.9 ± 1.5	42.2 ± 1.7	8.5	52.6 ± 2.1	57.0 ± 1.5	8.3
Nrf2$^{-/-}$	1.5	34.5 ± 1.3	37.0 ± 1.6	7.2	50.0 ± 2.0	52.1 ± 2.0	4.3
	3	34.9 ± 1.2	41.8 ± 1.4	19.5	52.1 ± 1.8	58.0 ± 2.1	11.2
	6	35.8 ± 1.4	47.7 ± 1.5^{A}	33.1	53.5 ± 1.7	67.5 ± 2.3^{A}	26.1

Values shown are the mean ± SEM for groups of 5 mice each. $^{A}P \leq 0.05$, significantly greater than the CS-exposed (6 months) *Nrf2*$^{+/+}$ mice.

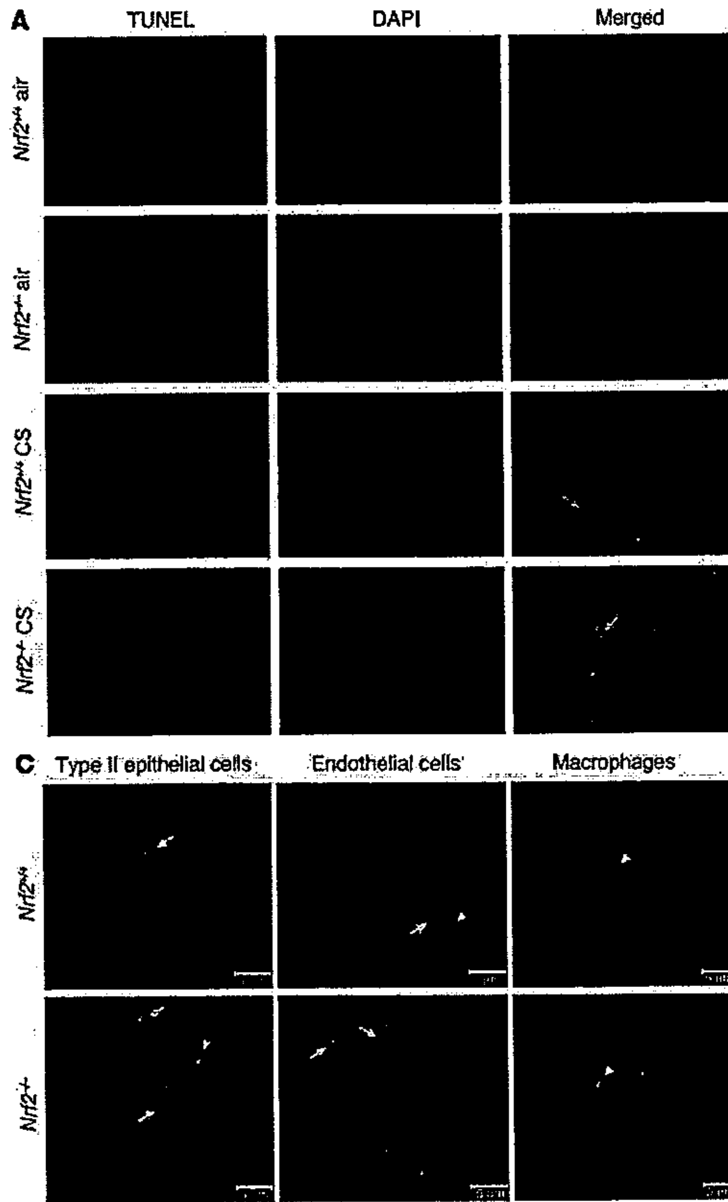

Figure 2
Cigarette smoke exposure causes lung cell apoptosis as assessed by TUNEL in $Nrf2^{-/-}$ lungs. (**A**) Lung sections ($n = 5$ per group) of room air– or CS-exposed (6 months) $Nrf2^{+/+}$ or $Nrf2^{-/-}$ mice were subjected to TUNEL (left column) and DAPI stain (middle column). Merged images are shown in the right column. CS-exposed $Nrf2^{-/-}$ mice show abundant TUNEL-positive cells (arrows) in the alveolar septa. Magnification, ×20. (**B**) Quantification of TUNEL-positive cells (per 1,000 DAPI-stained cells). The number of TUNEL-positive cells was significantly higher in the CS-exposed $Nrf2^{-/-}$ mice as compared with their wild-type counterparts ($^*P \leq 0.05$). Values represent mean ± SEM. (**C**) Identification of apoptotic (TUNEL-positive) type II epithelial cells (left column), endothelial cells (middle column), and alveolar macrophages (right column) in the lungs of CS-exposed (6 months) $Nrf2^{+/+}$ and $Nrf2^{-/-}$ mice. Type II epithelial cells, endothelial cells, and alveolar macrophages were detected with anti-SpC, anti-CD34, and anti–Mac-3 antibodies, respectively, as outlined in Methods. Nuclei were detected with DAPI (blue). Shown are the merged images, with colocalization (yellow arrows) of cell-specific markers (cytoplasmic red signal) and apoptosis (nuclear green + blue DAPI signal, resulting in a lavender-like signal); non-apoptotic (TUNEL-negative) cells with positive cell specific marker (red signal) are highlighted with a red arrow. TUNEL-positive apoptotic cells lacking a cell-specific marker are highlighted by white arrowheads. The majority of TUNEL-positive cells consisted of endothelial and type II epithelial cells, whereas most alveolar macrophages were TUNEL negative. Scale bars: 5 μm.

diameter (Table 1), highlighting the intrinsic resistance of $Nrf2^{+/+}$ ICR mice to CS-induced pulmonary emphysema.

Apoptosis assays. To determine whether chronic exposure to CS (6 months) induced apoptosis of alveolar septal cells in vivo, we conducted TUNEL on lung sections from air- and CS-exposed mice. Labeling of DNA strand breaks in situ by fluorescent TUNEL demonstrated a higher number of TUNEL-positive cells in the alveolar septa of CS-exposed $Nrf2^{-/-}$ mice (154.27 TUNEL-positive cells per 1,000 DAPI-positive cells) than in CS-exposed $Nrf2^{+/+}$ mice (26.42 TUNEL-positive cells per 1,000 DAPI-positive cells) or in air-exposed $Nrf2^{-/-}$ or $Nrf2^{+/+}$ mice (Figure 2, A and B). Double staining of the TUNEL-labeled lung sections (Figure 2C) with antibody to surfactant protein C (SpC) to label type II epithelial cells, anti-CD34 to label endothelial cells, and anti–Mac-3 to label macrophages revealed the occurrence of apoptosis, predominantly in endothelial ($Nrf2^{-/-}$ = 52 ± 3.6 vs. $Nrf2^{+/+}$ = 8 ± 1.8 TUNEL-positive and CD34-positive cells per 1,000 DAPI-positive alveolar cells) and type II epithelial cells ($Nrf2^{-/-}$ = 43 ± 4.3 vs. $Nrf2^{+/+}$ = 6 ± 0.96 TUNEL-positive and SpC-positive cells per 1,000 DAPI-positive alveolar cells) in the lungs of CS-exposed $Nrf2^{-/-}$ mice when compared with $Nrf2^{+/+}$ mice. Most alveolar macrophages in CS-exposed lungs did not show evidence of apoptosis ($Nrf2^{-/-}$ = 5 ± 0.42 Mac-3-positive cells per 1,000 DAPI-positive cells vs. $Nrf2^{+/+}$ = 3 ± 0.96 Mac-3-positive cells per 1,000 DAPI-positive cells).

Immunohistochemical analysis showed a higher number of caspase-3–positive cells in the alveolar septa of CS-exposed $Nrf2^{-/-}$ mice (4.83 active caspase-3–positive cells/mm alveolar length) than in CS-exposed $Nrf2^{+/+}$ mice (1.09 active caspase-3–positive cells/mm alveolar length). Lung sections from the air-exposed control $Nrf2^{-/-}$ and wild-type mice showed few or no caspase-3–posi-

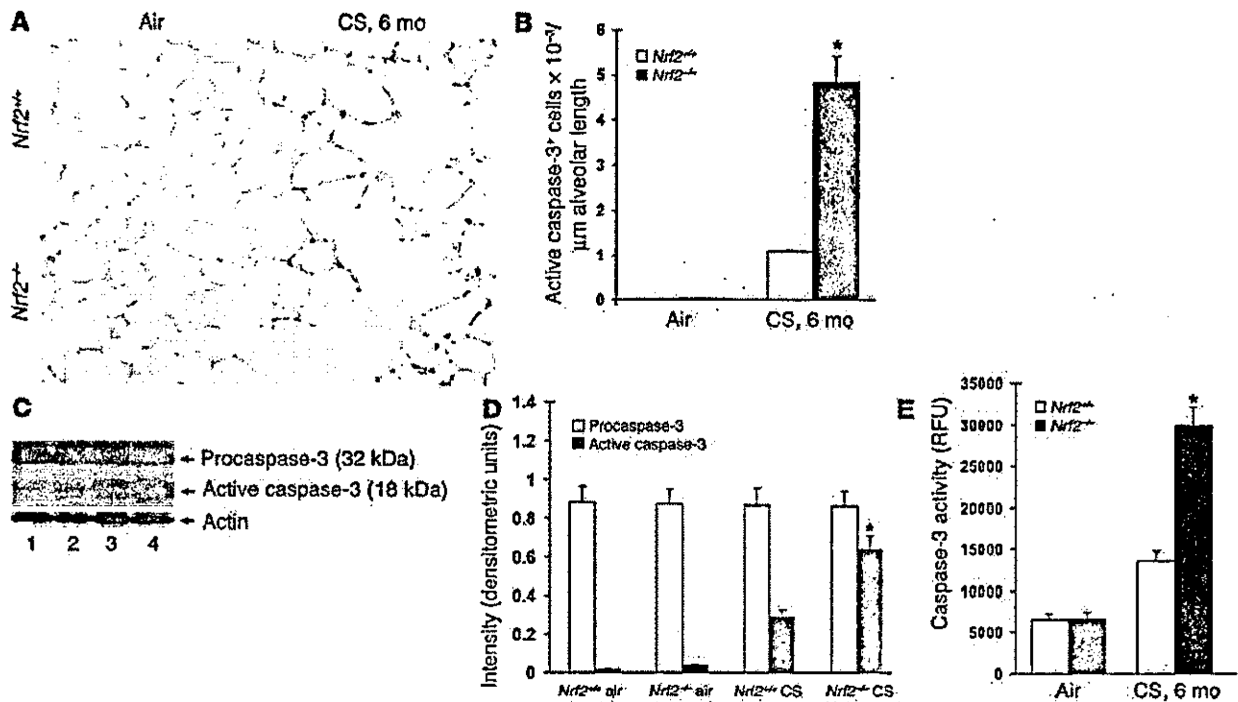

Figure 3

CS treatment leads to activation of caspase-3 in *Nrf2*$^{-/-}$ lungs. (A) Active caspase-3 expression in lung sections from CS-exposed (6 months) *Nrf2*$^{+/+}$ and *Nrf2*$^{-/-}$ mice. CS-exposed *Nrf2*$^{-/-}$ mice show increased numbers of caspase-3–positive cells in the alveolar septa (n = 5 per group). Magnification, ×40. (B) Number of caspase-3–positive cells in the lungs of air- and CS-exposed mice. Caspase-3–positive cells were significantly higher in the lungs of CS-exposed *Nrf2*$^{-/-}$ mice. (C) Increased expression of the 18-kDa active form of caspase-3 in lungs of CS-exposed (6 months) *Nrf2*$^{-/-}$ mice (Western blot; lanes 1 and 3: air- and CS-exposed *Nrf2*$^{+/+}$ mice, respectively; lanes 2 and 4: air- and CS-exposed *Nrf2*$^{-/-}$ mice, respectively). (D) Quantification of procaspase-3 and active caspase-3 obtained in Western blots of air- or CS-exposed *Nrf2*$^{+/+}$ and *Nrf2*$^{-/-}$ lungs. Values are represented as mean ± SEM. (E) Caspase-3 activity in the lungs of air- or CS-exposed (6 months) *Nrf2*$^{+/+}$ and *Nrf2*$^{-/-}$ mice. Caspase-3 activity was significantly higher in the lungs of CS-exposed *Nrf2*$^{-/-}$ mice than in the lungs of their wild-type counterparts (n = 3 per group). Values (relative fluorescence units [RFU]) are represented as mean ± SEM. *$P \leq 0.05$ vs. CS-exposed *Nrf2*$^{+/+}$ mice.

tive cells (Figure 3, A and B). Enhanced activation of caspase-3 in *Nrf2*$^{-/-}$ lungs exposed to CS for 6 months was further documented by the increased detection of the 18-kDa active caspase-3 peptide in whole-lung lysates (increase in *Nrf2*$^{-/-}$ mice was 2.3-fold that of CS-exposed *Nrf2*$^{+/+}$ mice; Figure 3, C and D), as well as by increased caspase-3 enzymatic activity (increase in activity in *Nrf2*$^{-/-}$ mice was 2.1-fold that of CS-exposed *Nrf2*$^{+/+}$ mice; Figure 3E).

Marker of oxidative stress in the lungs. Immunohistochemical staining with anti-8-oxo-7,8-dihydro-2′-deoxyguanosine (anti-8-oxo-dG) antibody was used to assess oxidative stress in both *Nrf2*$^{-/-}$ and *Nrf2*$^{+/+}$ lungs after inhalation of CS. A small number of alveolar septal cells (1.78 cells/mm alveolar length) exhibited staining for 8-oxo-dG in lung sections from the *Nrf2*$^{+/+}$ mice, whereas significantly more (16.8 cells/mm alveolar length) were stained in the *Nrf2*$^{-/-}$ mice (Figure 4, A and B). Lung sections from air-exposed *Nrf2*$^{+/+}$ and *Nrf2*$^{-/-}$ mice showed few or no 8-oxo-dG–positive cells. Immunostaining with normal mouse IgG antibody did not show any IgG-reactive cells in the lungs of air- or CS-exposed mice (Figure 4C). These results indicate that exposure to CS for 6 months enhanced oxidative damage to the lungs of the *Nrf2*-disrupted mice.

Inflammatory cells in the lungs. Analysis of differential cell counts in the bronchoalveolar lavage (BAL) fluid revealed a significant increase in the number of total inflammatory cells in the lungs of CS-exposed (1.5 or 6 months) *Nrf2*$^{+/+}$ and *Nrf2*$^{-/-}$ mice when compared to their respective air-exposed control littermates (Figure 5A). However, the total number of inflammatory cells in BAL fluid from the CS-exposed *Nrf2*$^{-/-}$ mice was significantly higher than in CS-exposed wild-type mice. Among the inflammatory cell population, macrophages were the predominant cell type, constituting as much as 87–90% of the total inflammatory cell population in the BAL fluid of both genotypes exposed to CS. Other inflammatory cells such as polymorphonuclear leukocytes, eosinophils, and lymphocytes constituted 10–13% of the total inflammatory cells in the BAL fluid of both genotypes. Immunohistochemical staining of the lung sections with Mac-3 antibody revealed the presence of an increased number of macrophages (Figure 5, B and C) in the lungs of CS-exposed *Nrf2*$^{-/-}$ mice at 6 months (4.54 Mac-3–positive cells/mm alveolar length) when compared with lungs of their wild-type counterparts (2.27 Mac-3–positive cells/mm alveolar length). However, the immunohistochemical staining did not show any significant difference in the number of alveolar macrophages in the lungs of air-exposed *Nrf2*$^{+/+}$ (0.96 Mac-3–positive cells/mm alveolar length) and *Nrf2*$^{-/-}$ mice (1.18 Mac-3–positive cells/mm alveolar length). There were significantly fewer neutrophils and lymphocytes than there were macrophages. There were 0.92 versus 0.49 neutrophils and 0.78 versus 0.43 lymphocytes per millimeter alveolar length in CS-exposed *Nrf2*$^{-/-}$ and wild-type mice, respectively (Supplemental Figure 3, A–D).

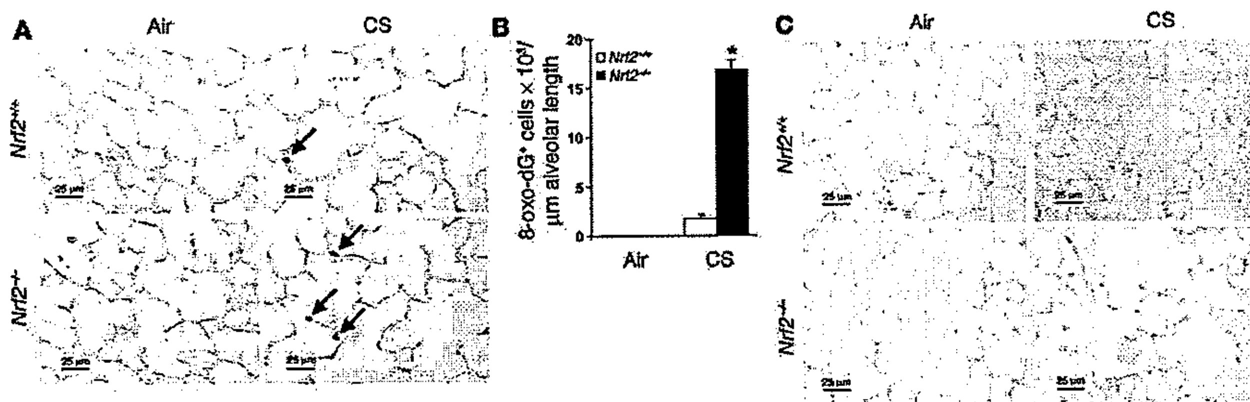

Figure 4
Increased sensitivity of *Nrf2*–/– mice to oxidative stress after CS exposure. (**A**) Immunohistochemical staining for 8-oxo-dG in lung sections from the mice exposed to CS (6 months) ($n = 5$ per group). Lung sections from the CS-exposed *Nrf2*–/– mice show increased staining for 8-oxo-dG (indicated by arrows) when compared with lung sections from CS-exposed *Nrf2*+/+ mice and the respective air-exposed control mice. Magnification, ×40. (**B**) Quantification of 8-oxo-dG–positive alveolar septal cells in lungs after 6 months of CS exposure. The number of cells that reacted with anti–8-oxo-dG antibody was significantly higher in the lung tissues of the CS-exposed *Nrf2*–/– mice than in the lung tissues of the CS-exposed *Nrf2*+/+ mice and air-exposed control mice. Values (positive cells/mm alveolar length) represent mean ± SEM. $^*P \le 0.05$ vs. CS-exposed *Nrf2*+/+ mice. (**C**) Immunohistochemical staining with normal mouse-IgG1 antibody in lung sections from air- or CS-exposed *Nrf2*+/+ and *Nrf2*–/– mice. Magnification, ×40. Scale bars: 25 µm.

Activation of Nrf2 in the lungs of Nrf2+/+ *mice.* An electrophoretic mobility shift assay (EMSA) was used to determine the activation and DNA binding activity of Nrf2 in the lungs in response to acute exposure of the mice to CS (5 hours). In response to CS, there was an increased binding of nuclear proteins isolated from the lungs of CS-exposed *Nrf2*+/+ mice to an oligonucleotide probe containing the ARE consensus sequence, as compared to the binding of nuclear proteins isolated from CS-exposed *Nrf2*–/– mice or air-exposed control mice. Supershift analysis with anti-Nrf2 antibody also showed the binding of Nrf2 to the ARE consensus sequence, suggesting the activation of Nrf2 in the lungs of *Nrf2*+/+ mice in response to CS exposure (Figure 6A). However, supershift analysis of the nuclear proteins from the lungs of CS-exposed *Nrf2*–/– mice with anti-Nrf2 antibody did not show any super-shifted band, consistent with the absence of Nrf2 in the ARE-nuclear protein complex.

Western blot analysis was performed to determine the nuclear accumulation of Nrf2 in the lungs in response to CS exposure. Immunoblot analysis (Figure 6B) showed increased levels of Nrf2 in the nuclei isolated from the lungs of CS-exposed *Nrf2*+/+ mice, suggesting the nuclear accumulation of Nrf2 in the lungs of wild-type mice in response to CS exposure. Increase of nuclear Nrf2 is needed for the activation of ARE and the transcriptional induction of various antioxidant genes.

Transcriptional induction of Nrf2-dependent genes. To uncover the Nrf2-dependent genes that may account for the emphysema-sensitive phenotype of the *Nrf2*–/– background, we examined the pulmonary expression profile of air- and CS-exposed (5 hours) mice by oligonucleotide microarray analysis using the Affymetrix mouse gene chip U74A. The complete gene expression data set is available at http://faculty.jhsph.edu/biswal2.xls. Table 2 lists the genes that were significantly upregulated in the lungs of *Nrf2*+/+ mice, but not in those of *Nrf2*–/– mice, in response to CS. The regions upstream of the transcription start site of these Nrf2-dependent genes were analyzed for the presence of putative AREs using the Genamics Expression 1.1 Pattern Finder Tool software. The location of the AREs in these Nrf2-dependent genes are also presented in Table 2. Nrf2 regulates about 50 antioxidant and cytoprotective genes. The majority of these Nrf2-regulated genes contain possible functional AREs in the genomic sequences upstream of their transcription start sites.

Validation of microarray data by Northern blot and enzyme assay. Validation of the microarray data was performed using the samples used in the arrays. Northern hybridization confirmed the transcriptional induction of genes involved in glutathione synthesis (glutamate cysteine ligase modifier subunit [GCLm]), NADPH regeneration (glucose-6-phosphate dehydrogenase [G6PDH]), detoxification of oxidative stress–inducing components of CS (by NADPH: quinone oxidoreductase-1 [NQO1], GST-α1, HO-1, thioredoxin reductase [TrxR], and peroxiredoxin-1 [Prx-1]) in the lungs of CS-exposed *Nrf2*+/+ but not *Nrf2*–/– mice (Figure 7A). Glutathione reductase (GSR) was also induced in CS-exposed *Nrf2*–/– mice; however, the magnitude of the induction was significantly higher in *Nrf2* wild-type mice than in *Nrf2*-disrupted mice. The increases in these induced genes (NQO1, 7.2-fold; GST-α1, 2-fold; heavy subunit of γ-GCS [γ-GCS(h)], 4.8-fold; TrxR, 4.8-fold; G6PDH, 2.2-fold; HO-1, 3.4-fold; GSR, 1.8 fold; Prx-1, 1.6-fold), as measured by Northern analysis, were comparable to those determined by microarray.

Enzyme assays of selected gene products (NQO1, GSR, Prx, glutathione peroxidase [GPx] and G6PDH) were carried out to determine the extent to which their transcriptional induction in the lung paralleled changes in their activities (Figure 7B). There were significant increases in the activities of all enzymes in the lungs of CS-exposed *Nrf2*+/+ mice when compared to those of CS-exposed *Nrf2*–/– mice as well as those of the air-exposed mice of both genotypes. Moreover, the basal activities of these enzymes were significantly lower in the air-exposed *Nrf2*-disrupted mice than in the air-exposed wild-type mice.

Discussion

Our findings indicate that Nrf2, as previously shown for MMP-12, is a critical determinant of susceptibility to emphysema caused by CS. Because oxidative stress has overarching effects on several impor-

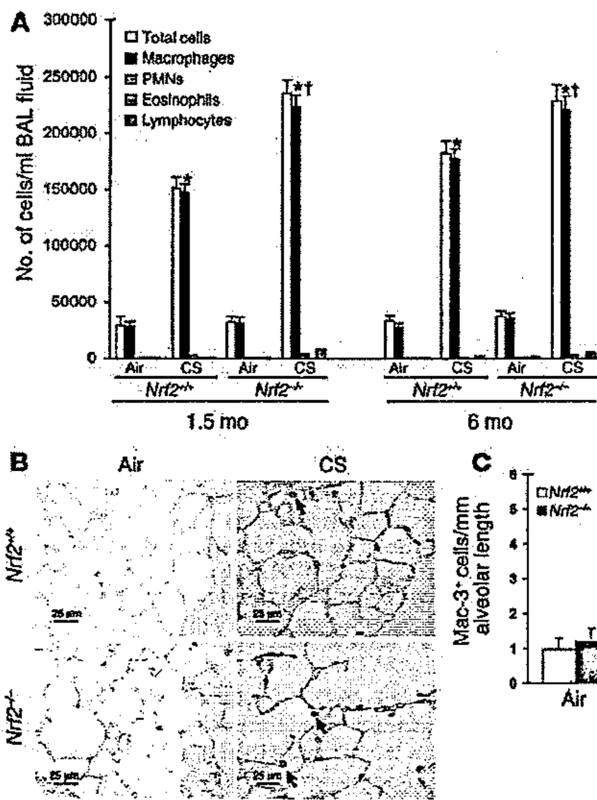

Figure 5

Increased inflammation in the lungs of CS-exposed $Nrf2^{-/-}$ mice. (**A**) Lavaged inflammatory cells from control and CS-exposed mice. The number of macrophages in BAL fluid collected from the CS-exposed (both 1.5 months and 6 months) $Nrf2^{-/-}$ mice was significantly higher than in the BAL fluid from CS-exposed $Nrf2^{+/+}$ mice and the respective age-matched control mice. Values represent mean ± SEM ($n = 8$). PMNs, polymorphonuclear leukocytes. $^{*}P \leq 0.05$ vs. control of the same genotype; $^{\dagger}P \leq 0.05$ across the genotypes in CS-exposed group. (**B**) Immunohistochemical detection of macrophages (arrows) in lungs of $Nrf2^{+/+}$ and $Nrf2^{-/-}$ mice exposed to CS for 6 months. Magnification, ×40. Scale bars: 25 μm. (**C**) Quantification of macrophages in lungs after 6 months of CS exposure. The lung sections from the CS-exposed $Nrf2^{-/-}$ mice showed significantly more macrophages than did those from wild-type counterparts exposed to CS ($^{**}P \leq 0.025$). However, there was no significant difference in the number of alveolar macrophages between the air-exposed $Nrf2^{+/+}$ and $Nrf2^{-/-}$ mice ($P > 0.9$).

tant mechanisms involved in CS-induced emphysema, particularly inflammation and apoptosis, Nrf2-induced gene expression may afford wide protection against the injurious effects of CS in the lung. The enhanced susceptibility of *Nrf2*-disrupted mice to CS-induced emphysema is remarkable, since the ICR parental strain (14) has been shown to be intrinsically resistant to CS-induced alveolar destruction and air space enlargement, as compared to susceptible strains such as C57BL/6J and DBA/2 (15). The higher levels of antioxidants and α1-antitrypsin in the lungs of ICR strain mice, as compared to those of susceptible strains, may contribute to this resistance (15).

We found that deletion of *Nrf2* resulted in increased alveolar inflammation, alveolar septal cell apoptosis involving predominantly endothelial and type II epithelial cells, enhanced alveolar oxidative stress, and ultimately more pronounced emphysema following exposure to CS, when compared with wild-type mice. Such broad lung pathogenic effects resulting from elimination of *Nrf2* indicate that, in CS-induced emphysema, oxidative stress regulates the intensity of alveolar inflammation, the extent of alveolar cell ap-optosis, and ultimately the rate of onset and severity of the emphysema. In fact, the increased severity of CS-induced emphysema caused by deletion of *Nrf2* in ICR mice is equivalent to that seen in MMP-12–competent C57Bl/6J mice (when compared to $MMP12^{-/-}$ mice) (7). Despite abundant evidence of the elevation of markers of pulmonary and systemic oxidative stress in chronic smokers, there is a paucity of mechanistic support for the centrality of oxidative stress in the pathogenesis

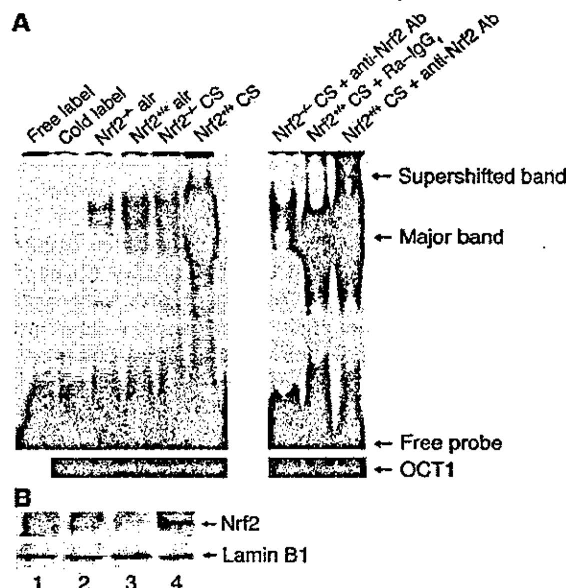

Figure 6

Activation of Nrf2 in CS-exposed $Nrf2^{+/+}$ lungs. (**A**) EMSA to determine the DNA binding activity of Nrf2. For gel shift analysis, 10 μg of nuclear protein from the lungs of air-and CS-exposed mice was incubated with the labeled human NQO1 ARE sequence and analyzed on a 5% non-denaturing polyacrylamide gel. For supershift assays, the labeled NQO1 ARE was first incubated with 10 μg of nuclear extract and then with 4 μg of anti-Nrf2 antibody for 2 hours. Nuclear protein of $Nrf2^{+/+}$ lungs showed increased binding to the ARE-containing sequence (lower arrow) after CS exposure, with a supershifted band caused by preincubation with anti-Nrf2 antibody, thus confirming the binding of Nrf2 to the ARE sequence (upper arrow). Ra–IgG_1, rabbit IgG_1. (**B**) Nuclear accumulation of Nrf2. Western blot analysis with anti-Nrf2 antibody showed the nuclear accumulation of the transcription factor Nrf2 in the lungs of $Nrf2^{+/+}$ mice in response to CS exposure (lanes 1 and 3: air-exposed $Nrf2^{-/-}$ and $Nrf2^{+/+}$ mice, respectively; lanes 2 and 4: CS-exposed $Nrf2^{-/-}$ and $Nrf2^{+/+}$ mice, respectively; lamin B1 was used as the loading control). Western blot analysis was carried out 3 times with the nuclear proteins isolated from the lungs of 3 different air- or CS-exposed $Nrf2^{+/+}$ and $Nrf2^{-/-}$ mice.

Table 2
Nrf2-dependent protective genes induced by CS in the lungs of *Nrf2* wild-type mice

Functional classification and gene accession no.	Gene	Fold change ± SE	ARE position
Antioxidants			
X56824 (X06985)	*Heme oxygenase 1*[A]	4.7 ± 0.4	–3928, –3992, –6007, –7103, –8978, –9007, –9036, –9065, –9500
U38261 (U10116)	*Superoxide dismutase 3*[B]	1.7 ± 0.4	–2362, –3171, –5282
X91864 (X68314)	*Glutathione peroxidase 2*[B]	2.7 ± 0.4	–44, –3600
U13705 (X58295)	*Glutathione peroxidase 3*[B]	1.4 ± 0.4	–7144, –9421
U85414 (M90656)	*Gamma glutamylcysteine synthase (catalytic)*[A]	7.6 ± 0.5	–3479, –3524, –5421
U95053 (L35546)	Gamma glutamylcysteine synthase (regulatory)[A]	7.3 ± 0.5	–44
AF090686 (M60396)	*Transcobalamine II*[B]	1.6 ± 0.3	–3751, –6382, –8236
L39879 (BC004245)	*Ferritin light chain 1*[A]	1.5 ± 0.3	–1379
AI118194 (X67951)	*Peroxiredoxin 1*[B]	1.5 ± 0.3	–78, –8413, –9652
AI851983 (X15722)	*Glutathione reductase*[B]	3.3 ± 0.4	–115, –9433
AB027565 (X91247)	*Thioredoxin reductase 1*[B]	4.3 ± 0.4	–121, –4326, –9521
Z11911 (X03674)	*Glucose-6-phosphate dehydrogenase*[B]	2.0 ± 0.3	–2504, –2109
AW120625 (U30255)	*Phosphogluconate dehydrogenase*[B]	2.1 ± 0.4	–757, –3963
Detoxification enzymes			
L06047(AF025887)	*Glutathione-S-transferase, α1*[B]	2.0 ± 0.3	NF
J03958 (M16594)	*Glutathione-S-transferase, α2*[A]	2.6 ± 0.3	–6662,– 6961, –7751
X65021	*Glutathione-S-transferase, α3*[B]	1.5 ± 0.3	No human homolog
AI843119 (U90313)	Glutathione-S-transferase, θ1[B]	2.0 ± 0.3	–255
X53451 (X06547)	Glutathione-S-transferase, π2[B]	3.1 ± 0.3	–71
J03952 (J03817)	*Glutathione-S-transferase GT8.7*[B]	1.6 ± 0.3	–1209
U12961 (J03934)	*NADPH: quinone reductase 1*[A]	9.3 ± 0.5	–527
U20257 (U09623)	Alcohol dehydrogenase 7 (class IV)[B]	2.8 ± 0.3	–2894
AV089850 (M74542)	Aldehyde dehydrogenase family 3, subfamily A1[B]	11.1 ± 0.8	–4223
U04204	*Aldo-keto reductase1, member B8*[B]	5.4 ± 0.5	No human homolog
AB017482 (AH005616)	*Retinol oxidase/Aldehyde oxidase*[B]	2.3 ± 0.4	–8579
AB025408 (AF112219)	*Esterase 10*[B]	3.4 ± 0.4	–4105, –4264
U16818 (J04093)	*UDP-glucuronosyl transferase*[B]	1.4 ± 0.3	–5431, –6221
AF061017 (AF061016)	*UDP-glucose dehydrogenase*[B]	1.5 ± 0.6	–3438
Protective proteins			
M64086 (AH002551)	*α1-antitrypsin proteinase inhibitor*[B]	4.7 ± 0.3	–4117
AB034693 (AB034695)	*Endomucin-1*[B]	1.5 ± 0.3	–2565
AW120711 (AF087870)	*Dnaj (HSP 40) homolog*[B]	1.9 ± 0.4	–155, –2797, –5320
D17666 (AU130219)	*Mitochondrial stress – 70 protein*[B]	1.6 ± 0.3	–2675, –3302
AF055638 (AF265659)	*GADD45G*[B]	2.4 ± 0.3	–327
U08210 (M16983)	*Tropoelastin*[B]	2.8 ± 0.9	NF
X04647 (X05562)	Procollagen type IV, α2[B]	1.9 ± 0.4	NF
Transcription factors			
AB009694 (AJ010857)	*mafF*[B]	2.6 ± 0.4	–3894, –6537, –8279, –8301, –8445
AF045160 (U81984)	*HIF-1α related factor*[B]	2.0 ± 0.4	–3855, –5091
Protein degradation			
AV305832 (M26880)	*Ubiquitin C*[B]	1.8 ± 0.4	–1393, –3755, –4481
AW121693 (AA020857)	Proteasome (prosome, macropain) 26S subunit, non ATPase, 1[B]	1.7 ± 0.3	NF
U40930 (BC017222)	*Seqestosome 1*[B]	2.9 ± 0.4	–360, –1328
Transporters			
M22998* (K03195)	*Solute carrier family 2*[B]	2.9 ± 0.2	–3351, –5111, –9304
X67056 (S70612)	*Glycine transporter*[B]	1.8 ± 0.3	–387, –8451
U75215 (BC026216)	*Neutral amino acid transporter mASCT1*[B]	3.8 ± 0.3	–3695, –8547
Phosphatases			
M97590 (AH003242)	*Tyrosine phosphatase (PTP1)*[B]	1.6 ± 0.3	–6045, –3232, –7029, –9884
X58289 (X5431)	Protein tyrosine phosphatase, receptor type B[B]	1.7 ± 0.4	–8166, –9561, –9662
Receptor			
AJ250490 (AJ001015)	*Receptor activity modifying protein 2*[B]	1.6 ± 0.3	–5023, –3455

AREs reported in the table are for human genes homologous to the respective mouse gene; the number in parenthesis refers to GenBank human accession number. To locate the AREs in each gene, we scanned 10-kb sequences upstream of the TSS in both strands using the ARE consensus sequence RTGAYNNNGCR as probe; the TSS for each gene was determined by following the Human Genome *build 34*, version 1 of the NCBI database. [A]Genes that have already been reported to have AREs and to be regulated by Nrf2; [B]Genes with the newly identified AREs using Genamics Expression 1.1 Pattern Finder Tool software (see Methods). NF, not found.

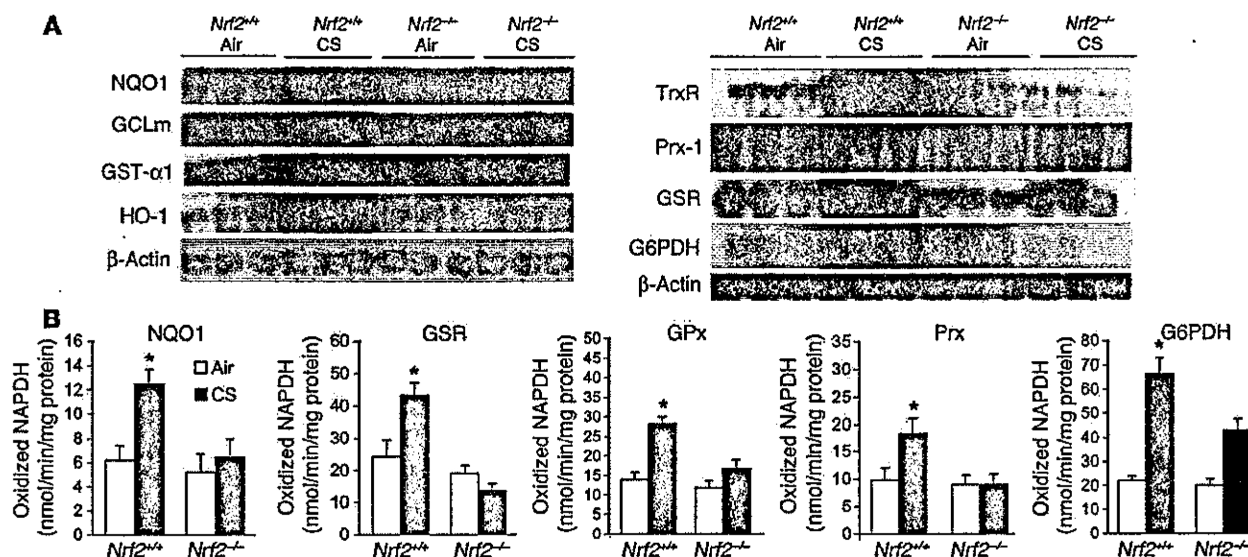

Figure 7

Validation of microarray data by Northern blot and enzyme assays. (A) Analysis of mRNA levels of NQO1, GCLm, GST-α1, HO-1, TrxR, Prx-1, GSR, and G6PDH in the lungs of *Nrf2*$^{+/+}$ and *Nrf2*$^{-/-}$ mice exposed to either air or CS ($n = 3$ per group). (B) Effect of CS on the specific activities of selected enzymes in the lungs of *Nrf2*$^{+/+}$ and *Nrf2*$^{-/-}$ mice. Values represent mean ± SE ($n = 3$ per group). $^*P \leq 0.05$ vs. control of the same genotype.

of CS-induced emphysema. An oxidative burden in the smoker's lungs is generated by the 4,700 chemical components present in CS and by the inflammatory cells that accumulate in the smoker's airways. This oxidative burden elicits a protective response that is dependent upon the ability of the lung cells to upregulate antioxidant defenses. The upregulation and activation of transcription factors such as Nrf2 might be one of these protective mechanisms. Prior and concomitant to airspace enlargement caused by CS exposure, there was an increased infiltration of inflammatory cells, predominantly macrophages, which may have contributed to the alveolar injury through the activity of their elastolytic enzymes, particularly MMP-12 (7). A decrease in the activity and levels of antiproteases might have followed the enhanced oxidative stress in our model and thus contributed to protease/antiprotease imbalance. However, future studies will determine the role of specific proteases in the development of emphysema in *Nrf2*$^{-/-}$ mice in response to CS.

In addition to inflammation, the lungs of *Nrf2*-disrupted mice show increased alveolar cell apoptosis when compared to wild-type lungs. Alveolar cell apoptosis has been progressively recognized as a critically important mechanism of alveolar septal destruction in emphysema. Apoptosis is required for emphysema caused by VEGF receptor inhibition and is sufficient to cause emphysema, as demonstrated in mice instilled intrabronchially with active caspase-3 (16). However, the contribution of alveolar cell apoptosis has not been addressed in animal models of CS-induced emphysema. Long-term exposure to CS resulted in increased apoptosis of endothelial and type II epithelial cells at the 6-month time point in the lungs of CS-exposed *Nrf2*$^{-/-}$ mice when compared with CS-exposed *Nrf2*$^{+/+}$ mice. Staining of the TUNEL-labeled lung sections with Mac-3 antibody showed the presence of few or no apoptotic macrophages in the lungs of CS-exposed *Nrf2*$^{+/+}$ or *Nrf2*$^{-/-}$ mice. Immunohistochemical staining, enzyme assay, and Western blot analysis have also revealed the increased number or activity of caspase-3 in the lungs of CS-exposed *Nrf2*$^{-/-}$ mice, suggesting the occurrence of excessive apoptosis. The presence of enhanced lung apoptosis in these *Nrf2*$^{-/-}$ mouse lungs might be related to enhanced oxidative stress, inflammation, or excessive lung proteolysis. Oxidative stress and apoptosis are part of a mutually interactive feedback loop in VEGF receptor blockade-induced emphysema (4). Furthermore, reactive oxygen and nitrogen species can modify and inactivate survival cell signaling molecules and cause apoptosis. Inflammation and protease/antiprotease imbalance may also promote apoptosis by means of activated T lymphocytes, which are increased in COPD and seem to correlate with the degree of emphysema (17) and the amount of unopposed leukocyte elastase (18), gelatinase, or collagenase (19) activity.

Consistent with a central role for Nrf2 in the upregulation of antioxidant defenses during CS-related stress, in *Nrf2*$^{-/-}$ mice exposed to CS, there was an enhanced formation of 8-oxo-dG, one of the most abundant DNA adducts in response to oxidative stress (20). The importance of Nrf2 in affording protection during oxidative stress has already been highlighted by the enhanced susceptibility of *Nrf2*$^{-/-}$ mice to hyperoxia (12, 21) and chemically induced lung injury (22). The majority of the genes that were significantly upregulated in the lungs of CS-exposed *Nrf2* wild-type mice, but not *Nrf2*-disrupted mice, have functions likely to confer protection against oxidative stress and inflammation.

Nrf2 — in association with several other proteins such as small maf proteins, c-jun, ARE binding protein-1, CBP/p300, and p160 family coactivators — binds to ARE, leading to transcriptional induction of target genes (23, 24). In response to CS exposure, there was an increased binding of nuclear proteins from the lungs of *Nrf2*$^{+/+}$ mice to the ARE sequence. This binding is presumably due to the interaction of nuclear proteins with the ARE, particularly of Nrf2 in the lungs of CS-exposed *Nrf2*$^{+/+}$ mice, as confirmed by the supershift analysis with anti-Nrf2 antibody. The slightly increased binding of nuclear proteins to ARE in knockout lung

extracts is probably due to the involvement of proteins other than Nrf2, since the supershift analysis failed to detect a complex of Nrf2 in *Nrf2*$^{-/-}$ lung extracts. Western blot analysis confirmed the nuclear accumulation of Nrf2 in the lungs of CS-exposed *Nrf2*$^{+/+}$ mice. Increased nuclear Nrf2 is critical for the activation of ARE and the transcriptional induction of various antioxidant genes.

Nrf2, in response to CS, regulates genes involved in two major redox systems, the glutathione and thioredoxin systems (25, 26). Enzymes involved in glutathione synthesis (γ-GCS catalytic and regulatory subunits), members of the GST family, GSR, GPx2, GPx3, and genes that constitute the thioredoxin system (TrxR and Prx-1) were all induced in the lungs of *Nrf2*$^{+/+}$ mice in response to CS. The members of these redox systems interact with various transducers and effector molecules to bring about antioxidant-specific responses. The regeneration of reduced Trx and glutathione by TrxR and GSR, respectively, utilizes NADPH as a reducing equivalent generated by G6PDH and phosphogluconate dehydrogenase, both of which are also induced in *Nrf2*$^{+/+}$ lungs. Prx-1 and GPx reduce hydroperoxides by utilizing two electrons provided by Trx and glutathione, respectively. In addition, GPx and peroxiredoxins have been shown to play a potential role in protection against peroxynitrite (27), a potent oxidant generated from the reaction of superoxide and nitrous oxide present in CS. Furthermore, the oxidized forms of GPx and peroxiredoxins are reduced back to their functional forms by Trx (28). These results suggest a cross talk between the thioredoxin and glutathione redox systems and the NADPH regenerating system.

Several GSTs, as well as UDP-glucuronosyl transferase (UGT) and NQO1, were selectively induced only in *Nrf2*$^{+/+}$ mice in response to CS. Various isoforms of GSTs and UGTs play important roles in the detoxification of tobacco smoke carcinogens such as 4-(methylnitrosamino)-1-(3-pyridyl)-1-butanone, benzo(a)pyrene and other polycyclic aromatic hydrocarbons that act as electrophiles and cause DNA damage and cytotoxicity (29, 30). NQO1 blocks redox cycling of polyaromatic hydrocarbons and benzoquinones present in CS (31), thereby reducing the levels of ROS and presumably 8-oxo-dG. Various enzymes, including aldehyde dehydrogenase and aldo-keto reductase, which are involved in the detoxification of reactive aldehydes such as acetaldehyde and acrolein, were selectively induced in the lungs of CS-exposed *Nrf2*$^{+/+}$ mice. HO-1, a critical enzyme involved in protection against oxidant-mediated cellular injury, as well as the iron-sequestering protein ferritin light chain 1, which prevents uncontrolled surges in the intracellular free concentration of the highly reactive yet poorly soluble ferric iron (32, 33), were induced only in the lungs of CS-exposed *Nrf2*$^{+/+}$ mice. Reduction of ferric iron by superoxide can generate reactive hydroxyl radicals via the Fenton reaction. Superoxide dismutase 3, the major extracellular antioxidant enzyme in the lung that attenuates ROS-mediated lung cell injury and inflammation, is also selectively upregulated in *Nrf2*$^{+/+}$ mice in response to CS (34). CS also induced heat shock proteins such as HSP40 and mitochondrial stress-70 protein, as well as ubiquitin C, a protein involved in the degradation of oxidized proteins. Other Nrf2-regulated genes included the DNA damage repair protein GADD45G, lung structural proteins such as tropoelastin and procollagen type IV, α2, and endomucin-1, sequestosome 1, MafF, HIF-1α–related factor and α1-antitrypsin proteinase inhibitor. Mutations in the α1-antitrypsin proteinase inhibitor have been associated with an increased risk of COPD (35). Furthermore, we have located one or more AREs in the upstream regions of most of these differentially expressed genes, indicating the possibility of a direct role for Nrf2 in their transcriptional induction.

Taken together, these results provide a clear link between a defective response of the transcription factor Nrf2 and several lung problems: excessive oxidative stress, increased apoptosis, inflammation, and worsened emphysema. Nrf2 is activated in response to CS in the lungs of wild-type mice, leading to transcriptional induction of target genes that might provide resistance against the development of emphysema. Conversely, a lack of responsiveness of the Nrf2 pathway confers susceptibility to severe emphysema due to CS exposure in this model. The identification of Nrf2 as a determinant of susceptibility can have wide implications in the area of tobacco smoke–related lung diseases, where oxidative stress and inflammation play important roles.

Methods

Antibodies and reagents. We used the following antibodies and reagents: anti-caspase-3 polyclonal antibody for immunohistochemistry (Idun Pharmaceuticals); biotinylated anti-mouse IgG, peroxidase-conjugated streptavidin, Vectashield HardSet mounting medium, and RTU HRP-avidin complex (Vector Laboratories); rabbit anti-SpC antibody (Chemicon International Inc.); rat anti-mouse Mac-3 antibody (BD Biosciences); anti-rabbit Texas red antibody, streptavidin-Texas red conjugated complex, and DAPI (Molecular Probes Inc.); biotinylated rabbit anti-mouse secondary antibody (DakoCytomation); octamer transcription factor 1 (OCT1) and CaspACE Assay kit (Promega Corp.); leupeptin, pepstatin A, and normal mouse IgG_1 (Sigma-Aldrich); rat anti-mouse neutrophil antibody (Serotec); actin and anti-mouse CD45R primary antibody (Santa Cruz Biotechnology Inc.); rabbit anti-caspase-3 antibody for Western blot (Cell Signaling Technology Inc.); anti-CD34 and anti-lamin B1 antibody (Zymed Laboratories Inc.); and CH11 monoclonal antibody (Beckman Coulter Inc.).

Animals and care. Nrf2-deficient ICR mice were generated as described (14). Mice were genotyped for *Nrf2* status by PCR amplification of genomic DNA extracted from blood (36). PCR amplification was carried out using 3 different primers: 5′-TGGACGGGACTATTGAAGGCTG-3′ (sense for both genotypes), 5′-CGCCTTTTCAGTAGATGGAGG-3′ (antisense for *Nrf2*$^{+/+}$ mice), and 5′-GCGGATTGACCGTAATGGGATAGG-3′ (antisense for LacZ) (36). Mice were fed AIN-76A diet (Harlan Teklad) and had access to water ad libitum; they were housed under controlled conditions (23 ± 2°C; 12-hour light/dark cycles). All experimental protocols conducted on the mice were performed in accordance with the standards established by the US Animal Welfare Acts, as set forth in NIH guidelines and in the Policy and Procedures Manual of the Johns Hopkins University Animal Care and Use Committee.

Exposure to CS. The CS machine for smoke exposure was similar to the one used by Witschi et al. (37). However, the exposure regimen in terms of chamber atmosphere and duration of CS exposure was considerably more intense. At 8 weeks of age, the mice were divided into four groups (n = 40 per group): control *Nrf2* wild-type mice, experimental *Nrf2* wild-type mice, control *Nrf2*-disrupted mice, and experimental *Nrf2*-disrupted mice. The control groups were kept in a filtered air environment, and the experimental groups were subjected to CS for various time periods. CS exposure was carried out (7 hours/day, 7 days/week for up to 6 months) by burning 2R4F reference cigarettes (2.45 mg nicotine per cigarette; purchased from the Tobacco Research Institute, University of Kentucky) using a smoking machine (Model TE-10, Teague Enterprises). Each smoldering cigarette was puffed for 2 seconds, once every minute for a total of 8 puffs, at a flow rate of 1.05 l/min, to provide a standard puff of 35 cm^3. The smoke machine was adjusted to produce a mixture of sidestream smoke (89%) and mainstream smoke (11%) by burning five cigarettes at

one time. Chamber atmosphere was monitored for total suspended particulates and carbon monoxide, with concentrations of 90 mg/m^3 and 350 ppm, respectively.

Morphologic and morphometric analyses. After exposure to CS for various time periods (1.5, 3, and 6 months), the mice (n = 5 per group) were anesthetized with halothane (Halocarbon Laboratories) and the lungs were inflated with 0.5% low-melting agarose at a constant pressure of 25 cm as previously described (38). The inflated lungs were fixed in 10% buffered formalin and embedded in paraffin. Sections (5 μm) were stained with H&E. Mean alveolar diameter, alveolar length, and mean linear intercepts were determined by computer-assisted morphometry with Image Pro Plus software (Media Cybernetics). The lung sections in each group were coded, and representative images (15 per lung section) were acquired with a Nikon E800 microscope (lens magnification, ×20) by an investigator who was blind to the identity of the slides (4).

TUNEL assay. Apoptotic cells in the tissue sections from the agarose-inflated lungs were detected by the Fluorescein-FragEL DNA Fragmentation Detection Kit (Oncogene Research Products) according to the recommendations of the manufacturer. The lung sections (n = 5 per group) were stained with the TdT labeling reaction mixture and mounted with Fluorescein-FragEL mounting medium (Oncogene Research Products). DAPI and fluorescein were visualized at 330–380 nm and 465–495 nm, respectively. Overlapping DAPI in red and FITC in green create a yellow, apoptotic-positive signal. Images (15 per lung section) of the lung sections were acquired with a Nikon E800 microscope (lens magnification, ×20). In each image, the number of DAPI-positive (red) and apoptotic cells (yellow) were counted manually. Apoptotic cells were normalized by the total number of DAPI-positive cells.

Identification of alveolar apoptotic cell populations in the lungs. To identify the different alveolar cell types undergoing apoptosis in the lungs, we performed fluorescent TUNEL labeling in the lung sections from the air- and CS-exposed (6 months) *Nrf2*$^{+/+}$ and *Nrf2*$^{-/-}$ mice, using the Fluorescein-FragEL DNA Fragmentation Detection Kit (Oncogene Research Products). To identify the apoptotic type II epithelial cells in the lungs after TUNEL labeling, we incubated the lung sections first with an anti-mouse SpC antibody and then with an anti-rabbit Texas red antibody. Apoptotic endothelial cells were identified by incubating the fluorescent TUNEL-labeled sections first with the anti-mouse CD34 antibody and then with the biotinylated rabbit anti-mouse secondary antibody. The lung sections were rinsed in PBS and then incubated with the streptavidin–Texas red conjugated complex. The apoptotic macrophages in the lungs were identified by incubating the TUNEL-labeled lung sections first with the rat anti-mouse Mac-3 antibody and then with the anti-rat Texas red antibody. Finally, DAPI was applied to all lung sections, incubated for 5 minutes, washed, and mounted with Vectashield HardSet mounting medium (Vector Laboratories). DAPI and fluorescein were visualized at 330–380 nm and 465–495 nm, respectively. Images of the lung sections were acquired with the Nikon E800 microscope, lens magnification ×40.

Immunohistochemical localization of active caspase-3. Immunohistochemical staining of active caspase-3 was performed using anti–active caspase-3 antibody (39), and the active caspase-3–positive cells were counted with a macro using the Image Pro Plus program (Media Cybernetics) (4). The counts were normalized by the sum of the alveolar profiles, herein named as alveolar length, and expressed in μm or mm. Alveolar length correlates inversely with the mean linear intercept, that is, as the alveolar septa are destroyed, the mean linear intercept increases as total alveolar length decreases.

Caspase-3 activity assay. Caspase-3 activity was assessed using a fluorometric CaspACE Assay commercial kit (Promega Corp.) according to the manufacturer's instructions. Briefly, the frozen lung tissues were immediately homogenized with hypotonic lysis buffer (25 mM HEPES [pH 7.5], 5 mM $MgCl_2$, 5 mM EDTA, 5 mM DTT, 2 mM PMSF, 10 μg/ml pepstatin A, and 10 μg/ml leupeptin) using a mechanical homogenizer on ice and centrifuged at 12,000 g for 15 minutes at 4°C. The clear supernatant was collected and frozen in liquid nitrogen. The protein was quantified using Bradford's reagent (Bio-Rad). Lung supernatant containing 30 μg of protein was added to a reaction buffer (98 μl) containing 2 μl DMSO, 10 μl of 100 mM DTT, and 32 μl of caspase assay buffer in a 96-well flat-bottom microtiter plate (Corning-Costar Corp.). The reaction mixture was incubated at 30°C for 30 minutes. Then, 2 μl of 2.5 mM caspase-3 substrate (Ac-DEVD-AMC) was added to the wells and incubated for 60 minutes at 30°C. The fluorescence of the reaction was measured at an excitation wavelength of 360 nm and an emission wavelength of 460 nm. We used 30 μg of protein from anti-Fas antibody–treated Jurkat cells (treated with 1 μg CH11 monoclonal antibody per milliliter of RPMI medium containing 5 × 10^5 cells for 16 hours at 37°C) as a positive control. A caspase-3–specific inhibitor (2 μl of 2.5 mM DEVD-CHO) was used to show specificity of caspase-3 activity. The activity was below background levels after the addition of caspase-3 inhibitor. These experiments were performed in triplicate and repeated 3 times.

Immunohistochemical localization of 8-oxo-dG. For the immunohistochemical localization and quantification of 8-oxo-dG, lung sections (n = 5 per group) from the mice exposed to CS for 6 months were incubated with anti-8-oxo-dG antibody and stained using the Iso-IHC DAB kit (InnoGenex) using mouse antibodies. Normal mouse-IgG1 antibody was used as a negative control. The 8-oxo-dG–positive cells were counted with a macro (using Image Pro Plus), and the counts were normalized by alveolar length as described (4).

BAL and phenotyping. Immediately following exposure to CS for 1.5 months or 6 months, mice (n = 8 per group) were anesthetized with sodium pentobarbital. The BAL fluid collected from the lungs of the mice was centrifuged (500 g at 4°C), and the cell pellet was resuspended in PBS. The total number of cells in the lavage fluid was determined, and 2 × 10^4 cells were cytocentrifuged (Shandon Southern Products) onto glass slides and stained with Wright-Giemsa stain (Diff-Quik; Baxter Scientific Products). Differential cell counts were performed on 300 cells, according to standard cytologic techniques (40).

Immunohistochemical localization of inflammatory cells in the lungs. Macrophages were identified by the rat anti-mouse Mac-3 and secondary biotinylated anti-rat antibody immunostaining using the Vector RTU HRP-avidin complex with 3,3′-diaminobenzidine as the chromogenic substrate. The number of Mac-3–positive cells in the lung sections (n = 3 per group and 10 fields per lung section) were counted manually and normalized by alveolar length.

EMSA. EMSA was carried out according to a procedure described previously (41). For gel shift analysis, 10 μg of nuclear protein that had been prepared from the lungs of mice exposed to air or to CS for 5 hours was incubated with the labeled human NQO1 ARE, and the mixtures were analyzed on a 5% nondenaturing polyacrylamide gel. To determine the specificity of protein(s) binding to the ARE sequence, 50-fold excess of unlabeled competitor oligo (ARE consensus sequence) was incubated with the nuclear extract for 10 minutes prior to the addition of radiolabeled probe. For supershift analysis, the labeled NQO1 ARE was first incubated for 30 min with 10 μg of nuclear proteins and then with 4 μg of anti-Nrf2 antibody for 2 hours. Normal rabbit IgG_1 (4 μg) was used as a control for the supershift assay. The mixtures were separated on native polyacrylamide gel and developed by autoradiography. The P^{32}-labeled consensus sequence for OCT1 was used as a control for gel loading. The EMSA was performed 3 times with the nuclear proteins isolated from 3 different air- or CS-exposed *Nrf2*$^{+/+}$ and *Nrf2*$^{-/-}$ mice.

Western blot analysis. Western blot analysis was performed according to previously published procedures (41). To determine the nuclear accumu-

lation of Nrf2, we used 10% SDS-PAGE to separate 50 μg of the nuclear proteins isolated from the lungs of air- or CS-exposed (5 hours) *Nrf2*$^{+/+}$ and *Nrf2*$^{-/-}$ mice. Then, we electrophoretically transferred them onto a PVDF membrane (Millipore). The membranes were blocked with 5% (w/v) BSA in Tris-buffered saline (20 mM Tris/HCl [pH 7.6] and 150 mM NaCl) with 0.1% [v/v] Tween-20 for 2 hours at room temperature, and then incubated overnight at 4°C with polyclonal rabbit anti-Nrf2 antibody, followed by incubation with HRP-conjugated secondary antibody. The blots were developed using an enhanced chemiluminescence Western blotting detection kit (Amersham Biosciences). Then, the blots were stripped and reprobed with anti-lamin B1 antibody.

To identify the active caspase-3, the lung tissues (n = 3) were homogenized with the lysis buffer (containing 50 mM Tris/HCl [pH 8.0], 150 mM NaCl, 0.5% (v/v) Nonidet P40, 2 mM EDTA, and a protease inhibitor cocktail) on ice using a mechanical homogenizer. Following centrifugation at 12,000 g for 15 minutes, the protein concentration of the supernatant was determined using Bradford's reagent. Equal amounts of protein (30 μg) were resolved on 15% SDS-PAGE and transferred onto a PVDF membrane (Millipore). The membranes were incubated with rabbit anti-caspase-3 antibody and then with secondary anti-rabbit antibody linked to HRP conjugate. The blots were developed using the enhanced chemiluminescence Western blotting detection kit (Amersham Biosciences). Thereafter, blots were stripped and reprobed with antibodies to actin. Western blot was performed thrice with protein extracts from 3 different air- or CS- exposed (6 months) *Nrf2*$^{+/+}$ and *Nrf2*$^{-/-}$ mice. Band intensities of procaspase-3 and active caspase-3 of the 3 blots were determined using NIH Image-Pro Plus software. Values are represented as mean ± SEM.

Transcriptional profiling using oligonucleotide microarrays. Lungs were excised from control (air-exposed) and CS-exposed (5 hours) mice (n = 3 per group) and processed for total RNA extraction using the TRIzol reagent (Invitrogen). The isolated RNA was used for gene expression profiling with Murine Genome U74A version 2 arrays (Affymetrix) using procedures described earlier (42). To identify the differentially expressed transcripts, pairwise comparison analyses were carried out with the Data Mining Tool 3.0 program (Affymetrix). Only those differentially expressed genes that appeared in at least 6 of the 9 comparisons and showed a change of more than 1.4-fold were selected. In addition, the Mann-Whitney pairwise comparison test was performed to rank the results by concordance as an indication of the significance ($P \leq 0.05$) of each identified change in gene expression. Genes which were upregulated only in the lungs of wild-type mice in response to CS were selected and used for the identification of AREs in their upstream sequence.

Identification of AREs in Nrf2-regulated genes. To identify the presence and location of AREs in Nrf2-dependent genes, the murine homologs of human genes were employed (Human Genome *build 34*, version 1, the National Center for Biotechnology Information [NCBI] database). For every gene, a 10-kb sequence upstream from the transcription start site (TSS) was used to search for AREs with the help of Genamics Expression 1.1 Pattern Finder Tool software (Genamics) using the primary core sequence of ARE (RTGAYNNNGCR) (43) as the probe. TSS for all the genes was determined by following the Human Genome *build 34*, version 1, of the NCBI database.

Northern blotting. Northern blotting was performed according to the procedure described earlier (42). In brief, 10 μg of total RNA isolated from the lungs of air- and CS-exposed (5 hours) mice (n = 3) was separated on 1.2% agarose gel, transferred to nylon membranes (NYTRAN Super Charge; Schleicher & Schuell), and ultraviolet-crosslinked. Full-length probes for NQO1, γ-GCS (regulatory subunit), GST-α1, HO-1, TrxR, Prx-1, GSR, G6PDH, and β-actin were generated by PCR from the cDNA of murine liver. These PCR products were radiolabeled with [α-^{32}P] cytidine triphosphate (CTP) and hybridized using QuickHyb solution (Stratagene) according to the manufacturer's protocol. After the films were exposed to the phosphoimager screen for 24 hours, hybridization signals were detected using a Bioimaging system (BAS1000, Fuji Photo Film). Quantification of mRNA was performed using Scion image analysis software (Scion Corporation). Levels of RNA were quantified and normalized for RNA loading by stripping and reprobing the blots with a probe for β-actin.

Enzyme activity assays. For measuring enzyme activity of selected genes, mice were exposed to CS for 5 hours and sacrificed after 24 hours. The lungs were excised (n = 3 per group) and processed as described (21) to measure the activities of NQO1, G6PDH, GPx, Prx, and GSR. GPx activity was measured according to the procedure of Flohe and Gunzler (44). NQO1 activity was determined using menadione as a substrate (45). The peroxidase activity of Prx was measured by monitoring the oxidation of NADPH as described (46). G6PDH activity was determined from the rate of glucose 6-phosphate-dependent reduction of NADP$^+$ (47). GSR activity was determined from the rate of oxidation of NADPH by using oxidized glutathione as substrate (48). Protein concentration was determined by using the Biorad reagent, with bovine serum albumin as the standard. The values for enzyme-specific activities are given as means ± SE. Student's t test was used to determine statistical significance.

Statistical analysis. Statistical analysis was performed by ANOVA, with the selection of the most conservative pairwise multiple comparison method using the program SigmaPlot 2000 (SPSS Inc.), and differences between groups were determined by Student's t test using the InStat program (GraphPad Software Inc.).

Acknowledgments

This work was supported by National Institute of Environmental Health Sciences Center grant P30 ES 03819; the Maryland Cigarette Restitution Fund (to S. Biswal); the Flight Attendant Research Institute (to S. Biswal); Alpha — 1 Foundation (to R.M. Tuder and I. Petrache); the American Thoracic Society and the American Lung Association (to I. Petrache); and NIH grants P50 CA058184, R01 66554 (to R.M. Tuder), and R01 CA94076 (to T.W. Kensler). We thank Wayne Mitzner for the total lung capacity measurements.

Received for publication January 23, 2004, and accepted in revised form September 7, 2004.

Address correspondence to: Shyam Biswal, Division of Toxicological Sciences, Department of Environmental Health Sciences, Bloomberg School of Public Health, Johns Hopkins University, Baltimore, Maryland 21205, USA. Phone: (410) 955-4728; Fax: (410) 955-0116; E-mail: sbiswal@jhsph.edu.

Chung Y. Cho and Rajesh K. Thimmulappa contributed equally to this work.

1. Mahadeva, R., and Shapiro, S.D. 2002. Chronic obstructive pulmonary disease * 3: Experimental animal models of pulmonary emphysema. *Thorax.* 57:908–914.
2. Petty, T.L. 2003. Definition, epidemiology, course, and prognosis of COPD. *Clin. Cornerstone.* 5:1–10.
3. Viegi, G., Scognamiglio, A., Baldacci, S., Pistelli, F., and Carrozzi, L. 2001. Epidemiology of chronic obstructive pulmonary disease (COPD). *Respiration.* 68:4–19.
4. Tuder, R.M., et al. 2003. Oxidative stress and apoptosis interact and cause emphysema due to vascular endothelial growth factor receptor blockade. *Am. J. Respir. Cell Mol. Biol.* 29:88–97.
5. Eriksson, S. 1964. Pulmonary emphysema and α1-antitrypsin deficiency. *Acta Med. Scand.* 175:197–205.
6. Joos, L., Pare, P.D., and Sandford, A.J. 2002. Genetic risk factors of chronic obstructive pulmonary disease. *Swiss Med. Wkly.* 132:27–37.
7. Hautamaki, R.D., Kobayashi, D.K., Senior, R.M.,

and Shapiro, S.D. 1997. Requirement for macrophage elastase for cigarette smoke-induced emphysema in mice. *Science.* 277:2002-2004.

8. Zheng, T., et al. 2000. Inducible targeting of IL-13 to the adult lung causes matrix metalloproteinase- and cathepsin-dependent emphysema. *J. Clin. Invest.* 106:1081-1093.
9. Horvath, I., et al. 2001. "Haemoxygenase-1 induction and exhaled markers of oxidative stress in lung diseases", summary of the ERS Research Seminar in Budapest, Hungary, September, 1999. *Eur. Respir. J.* 18:420-430.
10. MacNee, W., and Rahman, I. 2001. Is oxidative stress central to the pathogenesis of chronic obstructive pulmonary disease? *Trends Mol. Med.* 7:55-62.
11. Li, J., et al. 2003. Signaling intermediates required for NF-κB activation and IL-8 expression in CF bronchial epithelial cells. *Am. J. Physiol. Lung Cell Mol. Physiol.* 284:L307-L315.
12. Cho, H.Y., et al. 2002. Linkage analysis of susceptibility to hyperoxia. Nrf2 is a candidate gene. *Am. J. Respir. Cell Mol. Biol.* 26:42-51.
13. Nguyen, T., Sherratt, P.J., and Pickett, C.B. 2002. Regulatory mechanisms controlling gene expression mediated by the antioxidant response element. *Annu. Rev. Pharmacol. Toxicol.* 17:17.
14. Itoh, K., et al. 1997. An Nrf2/small Maf heterodimer mediates the induction of phase II detoxifying enzyme genes through antioxidant response elements. *Biochem. Biophys. Res. Commun.* 236:313-322.
15. Cavarra, E., et al. 2001. Effects of cigarette smoke in mice with different levels of alpha(1)-proteinase inhibitor and sensitivity to oxidants. *Am. J. Respir. Crit. Care Med.* 164:886-890.
16. Aoshiba, K., Yokohori, N., and Nagai, A. 2003. Alveolar wall apoptosis causes lung destruction and emphysematous changes. *Am. J. Respir. Cell Mol. Biol.* 28:555-562.
17. Finkelstein, R., Fraser, R.S., Ghezzo, H., and Cosio, M.G. 1995. Alveolar inflammation and its relation to emphysema in smokers. *Am. J. Respir. Crit. Care Med.* 152:1666-1672.
18. Trevani, A.S., et al. 1996. Neutrophil apoptosis induced by proteolytic enzymes. *Lab. Invest.* 74:711-721.
19. Segura-Valdez, L., et al. 2000. Upregulation of gelatinases A and B, collagenases 1 and 2, and increased parenchymal cell death in COPD. *Chest.* 117:684-694.
20. Kasai, H. 1997. Analysis of a form of oxidative DNA damage, 8-hydroxy-2'-deoxyguanosine, as a marker of cellular oxidative stress during carcinogenesis. *Mutat. Res.* 387:147-163.
21. Cho, H.Y., et al. 2002. Role of NRF2 in protection against hyperoxic lung injury in mice. *Am. J. Respir. Cell Mol. Biol.* 26:175-182.
22. Chan, K., and Kan, Y.W. 1999. Nrf2 is essential for protection against acute pulmonary injury in mice. *Proc. Natl. Acad. Sci. U. S. A.* 96:12731-12736.
23. Dhakshinamoorthy, S., and Jaiswal, A.K. 2000. Small maf (MafG and MafK) proteins negatively regulate antioxidant response element-mediated expression and antioxidant induction of the NAD(P)H:Quinone oxidoreductase1 gene. *J. Biol. Chem.* 275:40134-40141.
24. He, C.H., et al. 2001. Identification of activating transcription factor 4 (ATF4) as an Nrf2-interacting protein. Implication for heme oxygenase-1 gene regulation. *J. Biol. Chem.* 276:20858-20865.
25. Das, K.C., and White, C.W. 2002. Redox systems of the cell: possible links and implications. *Proc. Natl. Acad. Sci. U. S. A.* 99:9617-9618.
26. Casagrande, S., et al. 2002. Glutathionylation of human thioredoxin: a possible crosstalk between the glutathione and thioredoxin systems. *Proc. Natl. Acad. Sci. U. S. A.* 99:9745-9749.
27. Sies, H., and Arteel, G.E. 2000. Interaction of peroxynitrite with selenoproteins and glutathione peroxidase mimics. *Free Radic. Biol. Med.* 28:1451-1455.
28. Nordberg, J., and Arner, E.S. 2001. Reactive oxygen species, antioxidants, and the mammalian thioredoxin system. *Free Radic. Biol. Med.* 31:1287-1312.
29. Kim, P.M., and Wells, P.G. 1996. Genoprotection by UDP-glucuronosyltransferases in peroxidase-dependent, reactive oxygen species-mediated micronucleus initiation by the carcinogens 4-(methylnitrosamino)-1-(3-pyridyl)-1-butanone and benzo[a]pyrene. *Cancer Res.* 56:1526-1532.
30. Engel, L.S., et al. 2002. Pooled analysis and meta-analysis of glutathione S-transferase M1 and bladder cancer: a HuGE review. *Am. J. Epidemiol.* 156:95-109.
31. Dinkova-Kostova, A.T., and Talalay, P. 2000. Persuasive evidence that quinone reductase type 1 (DT diaphorase) protects cells against the toxicity of electrophiles and reactive forms of oxygen. *Free Radic. Biol. Med.* 29:231-240.
32. Vogt, B.A., Alam, J., Croatt, A.J., Vercellotti, G.M., and Nath, K.A. 1995. Acquired resistance to acute oxidative stress. Possible role of heme oxygenase and ferritin. *Lab. Invest.* 72:474-483.
33. Brittenham, G.M., et al. 2000. Clinical consequences of new insights in the pathophysiology of disorders of iron and heme metabolism. *Hematology (Am. Soc. Hematol. Educ. Program).* 39-50.
34. Folz, R.J., Abushamaa, A.M., and Suliman, H.B. 1999. Extracellular superoxide dismutase in the airways of transgenic mice reduces inflammation and attenuates lung toxicity following hyperoxia. *J. Clin. Invest.* 103:1055-1066.
35. Poller, W., et al. 1992. Mis-sense mutation of alpha 1-antichymotrypsin gene associated with chronic lung disease. *Lancet.* 339:1538.
36. Ramos-Gomez, M., et al. 2001. Sensitivity to carcinogenesis is increased and chemoprotective efficacy of enzyme inducers is lost in nrf2 transcription factor-deficient mice. *Proc. Natl. Acad. Sci. U. S. A.* 98:3410-3415.
37. Witschi, H., Espiritu, I., Maronpot, R.R., Pinkerton, K.E., and Jones, A.D. 1997. The carcinogenic potential of the gas phase of environmental tobacco smoke. *Carcinogenesis.* 18:2035-2042.
38. Kasahara, Y., et al. 2000. Inhibition of VEGF receptors causes lung cell apoptosis and emphysema. *J. Clin. Invest.* 106:1311-1319.
39. Kasahara, Y., et al. 2001. Endothelial cell death and decreased expression of vascular endothelial growth factor and vascular endothelial growth factor receptor 2 in emphysema. *Am. J. Respir. Crit. Care Med.* 163:737-744.
40. Saltini, C., et al. 1984. Accurate quantification of cells recovered by bronchoalveolar lavage. *Am. Rev. Respir. Dis.* 130:650-658.
41. Tirumalai, R., Rajesh Kumar, T., Mai, K.H., and Biswal, S. 2002. Acrolein causes transcriptional induction of phase II genes by activation of Nrf2 in human lung type II epithelial (A549) cells. *Toxicol. Lett.* 132:27-36.
42. Thimmulappa, R.K., et al. 2002. Identification of Nrf2-regulated genes induced by the chemopreventive agent sulforaphane by oligonucleotide microarray. *Cancer Res.* 62:5196-5203.
43. Wasserman, W.W., and Fahl, W.E. 1997. Functional antioxidant responsive elements. *Proc. Natl. Acad. Sci. U. S. A.* 94:5361-5366.
44. Flohe, L., and Gunzler, W.A. 1984. Assays of glutathione peroxidase. *Meth. Enzymol.* 105:114-121.
45. Prochaska, H.J., and Santamaria, A.B. 1988. Direct measurement of NAD(P)H:quinone reductase from cells cultured in microtiter wells: a screening assay for anticarcinogenic enzyme inducers. *Anal. Biochem.* 169:328-336.
46. Chae, H.Z., Kang, S.W., and Rhee, S.G. 1999. Isoforms of mammalian peroxiredoxin that reduce peroxides in presence of thioredoxin. *Meth. Enzymol.* 300:219-226.
47. Lee, C.Y. 1982. Glucose-6-phosphate dehydrogenase from mouse. *Meth. Enzymol.* 89:252-257.
48. Carlberg, I., and Mannervik, B. 1985. Glutathione reductase. *Meth. Enzymol.* 113:484-490.

Transcription Factor Nrf2 Is Essential for Induction of NAD(P)H:Quinone Oxidoreductase 1, Glutathione *S*-Transferases, and Glutamate Cysteine Ligase by Broccoli Seeds and Isothiocyanates[1,2]

Gail K. McWalter, Larry G. Higgins, Lesley I. McLellan, Colin J. Henderson, Lijiang Song,* Paul J. Thornalley,* Ken Itoh,† Masayuki Yamamoto,† and John D. Hayes[3]

*Biomedical Research Centre, Ninewells Hospital and Medical School, University of Dundee, Dundee DD1 9SY, Scotland, United Kingdom; *Disease Mechanisms and Therapeutics Research Group, Department of Biological Sciences, University of Essex, Essex CO4 3SQ, United Kingdom; †Centre for Tsukuba Advanced Research Alliance and Institute of Basic Medical Sciences, University of Tsukuba, Tsukuba 305-8577, Japan*

ABSTRACT Cruciferous vegetables contain glucosinolates that, after conversion to isothiocyanates (ITC), are capable of inducing cytoprotective genes. We examined whether broccoli seeds can elicit a chemoprotective response in mouse organs and rodent cell lines and investigated whether this response requires nuclear factor-erythroid 2 p45-related factor 2 (Nrf2). The seeds studied contained glucosinolate at 40 mmol/kg, of which 59% comprised glucoiberin, 19% sinigrin, 8% glucoraphanin, and 7% progoitrin. Dietary administration of broccoli seeds to *nrf2*$^{+/+}$ and *nrf2*$^{-/-}$ mice produced a ~1.5-fold increase in NAD(P)H:quinone oxidoreductase 1 (NQO1) and glutathione *S*-transferase (GST) activities in stomach, small intestine, and liver of wild-type mice but not in mutant mice; increased transferase activity was associated with elevated levels of GSTA1/2, GSTA3, and GSTM1/2 subunits. These seeds also increased significantly the level of glutamate cysteine ligase catalytic (GCLC) subunit in the stomach and the small intestine of *nrf2*$^{+/+}$ mice but not *nrf2*$^{-/-}$ mice. An aqueous broccoli seed extract was prepared for treatment of cultured cells that contained ITC at ~600 μmol/L, composed of 61% 3-methylsulfinylpropyl ITC, 30% sulforaphane, 4% allyl ITC, and 4% 3-butenyl ITC. This extract induced GSTA1/2, GSTA3, NQO1, and GCLC between 3-fold and 10-fold in mouse Hepa-1c1c7 and rat liver RL-34 cells. The broccoli seed extract affected increases in GSTA3, GSTM1, and NQO1 proteins in *nrf2*$^{+/+}$ mouse embryonic fibroblasts but not in *nrf2*$^{-/-}$ mouse embryonic fibroblasts. These experiments show that broccoli seeds are effective at inducing antioxidant and detoxication proteins, both in vivo and ex vivo, in an Nrf2-dependent manner. J. Nutr. 134: 3499S–3506S, 2004.

KEY WORDS: • *antioxidant response element* • *chemoprevention* • *glucosinolates* • *sulforaphane* • *myrosinase*

Individuals who have a high dietary intake of fruit and vegetables appear to have a lower risk of cancer (1). Among vegetables with anticarcinogenic properties, members of the Cruciferae family have been reported to protect against neoplastic disease at a variety of sites, such as the gastrointestinal tract and the lungs (2–6).

The cancer chemopreventive effect of cruciferous vegetables has been attributed to the fact that they contain high levels of glucosinolates (7,8). During food preparation and eating, these glucosinolates are hydrolyzed by the plant enzyme myrosinase to yield a complex number of breakdown products, including isothiocyanates (ITC),[4] thiocyanates, cyanides, nitriles, and epithio-containing compounds (7–9).

[1] Published in a supplement to *The Journal of Nutrition*. Presented as part of the International Research Conference on Food, Nutrition, and Cancer held in Washington, DC, July 15–16, 2004. This conference was organized by the American Institute for Cancer Research and the World Cancer Research Fund International and sponsored by BASF Aktiengesellschaft; Campbell Soup Company; The Cranberry Institute; Danisco USA Inc.; DSM Nutritional Products, Inc.; Hill's Pet Nutrition, Inc.; Kellogg Company; National Fisheries Institute; The Solae Company; and United Soybean Board. An educational grant was provided by The Mushroom Council. Guest editors for this symposium were Helen A. Norman, Vay Liang W. Go, and Ritva R. Butrum.

[2] Supported by grant 2000/11 from the World Cancer Research Fund and by grant G0000268 from the Medical Research Council of the UK (L.G.H.).

[3] To whom correspondence should be addressed.
E-mail: john.hayes@cancer.org.uk.

[4] Abbreviations used: AITC, allyl isothiocyanate; ARE, antioxidant response element; GCLC, glutamate cysteine ligase catalytic; GCLM, glutamate cysteine ligase modifier; GST, glutathione *S*-transferase; ITC, isothiocyanate; LC-MS/MS, liquid chromatography with triple quadrupole mass spectrometric detection; MEF, mouse embryonic fibroblast; MRM, multiple reaction monitoring; NQO1, NAD(P)H:quinone oxidoreductase 1; Nrf2, nuclear factor-erythroid 2 p45-related factor 2.

0022-3166/04 $8.00 © 2004 American Society for Nutritional Sciences.

Some of these breakdown products, and, in particular, ITCs can increase the levels of detoxication enzymes in rodent organs and in mouse, rat, and human cell lines (10–17). Inducible proteins include the drug-metabolizing enzymes aldo-keto reductase, NAD(P)H:quinone oxidoreductase 1 (NQO1), and glutathione S-transferase (GST). Increases in the levels of these detoxication enzymes would be expected to confer protection against chemical carcinogens such as benzo[*a*]pyrene, and, in experimental models, this prediction appears to hold true (14,18). Less well appreciated is the fact that glucosinolate breakdown products also induce antioxidant proteins, such as the glutamate cysteine ligase catalytic (GCLC) and glutamate cysteine ligase modifier (GCLM) subunits, that catalyze the rate-limiting step in the formation of reduced glutathione (19,20). They also induce glutathione reductase, ferritin, and glucose-6-phosphate dehydrogenase (20). Increases in the levels of detoxication enzymes and antioxidant proteins would be expected to protect against reactive oxygen species and the harmful metabolites they generate as a consequence of damaging cellular membranes, proteins, and nucleic acids (21).

Many genes encoding detoxication and antioxidant proteins are regulated by nuclear factor-erythroid 2 p45-related factor 2 (Nrf2) (22). This basic-region leucine zipper transcription factor mediates the transcriptional activation of genes in response to oxidative and electrophile stress. Under normal homeostatic conditions, Nrf2 protein has a short half-life, being targeted for proteasomal degradation by Keap1 (23–26). Oxidants and electrophiles interfere with Keap1-facilitated degradation of Nrf2, causing it to become more stable. This process involves oxidation, modification, or both, of cysteine residues 273 and 288 in Keap1 by the inducing compounds (27). Induction of NQO1, GST, GCLC, and GCLM genes by Nrf2 occurs through it being recruited to antioxidant response elements (ARE) in their gene promoters (28); Nrf2 binds the ARE as a heterodimer with small Maf proteins (29,30). Mice in which the *nrf2* gene has been disrupted by targeted homologous recombination have lower constitutive levels of NQO1 and GST proteins in liver and small intestine (19,31,32). Furthermore, $nrf2^{-/-}$ mice are either unable to respond or have a blunted response to the model cancer chemopreventive agent butylated hydroxyanisole (19,33,34).

Most investigations into the ability of plant chemicals to increase antioxidant gene expression used highly purified compounds as inducing agents (11–20). Thus, ITCs such as sulforaphane have been shown to increase NQO1 enzyme activity in the mouse liver Hepa-1c1c7 cell line (35). Frequently, it is unclear whether the concentration of phytochemical used in cell culture experiments is physiologically relevant and whether, because of limitations caused by bioavailability or disposition, the dose of chemical used can be achieved in target tissues in vivo. The question of whether extracts of cruciferous plants are as effective as purified phytochemicals at stimulating gene expression is seldom addressed.

In this study, we investigated whether broccoli seeds, either in the diet or as aqueous extracts, can affect induction of antioxidant and detoxication genes in vivo, in transformed cells, and in nontransformed cells. We also tested the hypothesis that Nrf2, through stimulating ARE-driven gene transcription, is essential for gene induction by broccoli-derived phytochemicals.

MATERIALS AND METHODS

Chemicals

Allyl ITC (AITC) and sulforaphane were obtained from Aldrich and LKT Laboratories, respectively. All other chemicals used were of the highest purity that was available from commercial suppliers.

Broccoli seeds

Broccoli seeds were purchased from Thompson and Morgan.

Processing of broccoli seeds for induction experiments

The broccoli seeds were processed at room temperature (20°C). Extracts were prepared by crushing 10 g seeds (dry weight), by pestle and mortar, to a fine powder. For mice feeding experiments, crushed broccoli seeds were added directly to powdered RM1 laboratory animal feed (SDS) at 15% by weight. For cell culture experiments, the broccoli seed powder was suspended in 3 volumes of distilled water and was mixed vigorously for 5 min. The suspension was centrifuged at 800 × *g* for 10 min before being filtered through a 0.2-μm sterile filter. Aliquots (1 mL) of the aqueous filtered extract were snap-frozen in liquid nitrogen and were stored at −70°C before use; the entire process from crushing the broccoli seeds to snap-freezing the filtered aqueous extract was completed within 30 min. The frozen extracts were thawed rapidly and diluted 1/1000 in 6 mL of medium for cell culture experiments that were conducted in 60-mm dishes.

Analysis of glucosinolates and ITCs in broccoli seeds

Glucosinolates and corresponding ITCs were identified by liquid chromatography with triple quadrupole MS detection (LC-MS/MS). Standard reference glucosinolates were isolated and purified from *Brassica* seeds by modification of published methods (36), and the related ITCs were prepared by myrosinase-catalyzed hydrolysis (37) and purified by preparative reversed-phase HPLC. The following glucosinolates were analyzed by LC-MS/MS: sinigrin, gluconapin, progoitrin, glucoiberin, glucoraphanin, glucoalyssin, and gluconasturtiin and their related ITCs—AITC, 3-butenyl ITC, 5-vinyloxazolidine-2-thione, 3-methylsulfinylpropyl ITC, sulforaphane, 5-methylsulfinylpentyl ITC, and phenethyl ITC, respectively.

Glucosinolates and ITCs were determined in broccoli seeds by initial heating at 110°C for 2 h (to inactivate myrosinase). The seeds were then ground to a fine powder, lipid was removed by extraction with chloroform, and the residual solid was extracted twice with 75% methanol at 75°C. The combined methanol extracts were concentrated by removal of solvent under reduced pressure, filtered (0.2 μm), spiked with authentic standard analytes, and analyzed by LC-MS/MS. For detection of ITCs in samples of seed extract and in culture medium, ITCs were extracted into dichloromethane and derivatized with ammonia (1.33 mol/L, 24 h at 20°C). The derivatized extracts were then evaporated under reduced pressure, reconstituted in 50% methanol, filtered (0.2 μm), spiked with authentic standard analytes, and analyzed by LC-MS/MS.

Glucosinolates were detected by negative ion electrospray multiple reaction monitoring (MRM), where the fragment ion was hydrogen sulfate (38). Derivatized ITCs were detected by positive ion electrospray MRM, where fragmentation involved loss of ammonia. For LC-MS/MS, the HPLC column was a 100 × 2.1-mm octadecyl silica Symmetry column with a 10 × 2.1-mm guard column (Waters). The flow rate was 0.2 mL/min. The eluent was 0.1% (v:v) trifluoroacetic acid in water, with linear gradients of methanol (0–10% for glucosinolates and 0–80% for ITCs) over 30 min. Source and desolvation temperatures were 120 and 350°C, and the gas flows for cone and desolvation were 150 and 550 L/h, respectively. The capillary voltage was 2.50 kV, and the cone voltage was set at 50 V. Argon gas pressure in the collision cell was 2.9×10^{-3} mbar. Programmed molecular ions, fragment ions, and collision energies were optimized to ±0.1 Da and ±1 eV for MRM detection. Glucosinolate and ITC analytes were quantified by standard addition analysis. Samples ana-

lyzed were spiked with 1–100 pmol glucosinolate and 2–100 pmol ITC. The limits of detection for glucosinolates were ≤0.4 pmol and, for ITCs, were ≤2 pmol. The interbatch coefficients of variation were <5%, and recoveries were 80–100%.

Mice feeding experiments

The Ethical Review Committee of the University of Dundee approved this program of work, and, throughout the study, mice were treated as advised by regulations contained in the Animals and Scientific Procedure Act (1986) of the United Kingdom. The $nrf2^{+/+}$ and $nrf2^{-/-}$ mice were obtained as described previously (33). The mice used in this study have been backcrossed over 6 generations onto a C57BL/6 genetic background. Female mice of between 9 and 14 wk of age were used in all studies. Mice were fed on standard RM1 laboratory feed. Mice were given free access to RM1 feed with broccoli seeds at 15% (by weight) for 7 d immediately before being killed. During the administration of crushed broccoli seed, mice were monitored daily by measurement of body weight. Once the period of feeding these phytochemicals was complete, the mice were killed by exposure to a rising concentration of CO_2. Organs were removed and snap-frozen immediately in liquid nitrogen before being stored at −70°C.

Cell culture

Mouse Hepa-1c1c7 cells (European Collection of Animal Cell Cultures) were maintained in minimal essential Eagle's medium, with the Alpha modification (Sigma) supplemented with 10% (v:v) heat-inactivated fetal bovine serum, 50 U/mL penicillin-streptomycin mixture, and L-glutamine at 2 mmol/L. Rat liver RL-34 cells [Japanese Cancer Research Resources Bank (Setagaya-ku)] were grown in Dulbecco's modified Eagle's medium (Life Technologies) supplemented as described above. Wild-type and Nrf2-null mouse embryonic fibroblasts (MEF) were prepared from $nrf2^{+/+}$ and $nrf2^{-/-}$ mouse lines as described by Tiemann and Deppert (39). These cells were maintained in tissue culture flasks coated with 0.1% (w:v) gelatin for 30 min before use and were grown in medium supplemented with 10 μg/L human recombinant epidermal growth factor, 1 × insulin-transferrin-selenium (Gibco), and 10% (v:v) fetal bovine serum. All cell lines were maintained at 37°C and 5% CO_2.

The RL-34, Hepa-1c1c7, and MEF cells were cultured in monolayers and were allowed to grow to 80% confluence in 60-mm dishes before exposure for 24 h to phytochemicals. AITC and sulforaphane were both used to treat cells at a dose of 5 μmol/L. The aqueous broccoli seed extract used to treat cells contained several ITCs, with the total level in the culture media amounting to 0.6 μmol/L.

Enzyme assays and Western blotting

NQO1 enzyme activity was estimated by measuring the dicoumarol-inhibitable fraction of dichlorophenol indophenol reductase activity. GST enzyme activity was measured using 1-chloro-2,4-dinitrobenzene. Western blotting using antibodies against NQO1; class Apha, Mu, and Pi GST isoenzymes; and GCLC subunits was conducted as reported previously (12,19,31).

DNA transfection and luciferase reporter gene assays

Transfection and ARE-reporter gene assays were performed in Hepa-1c1c7 cells. The wild-type mouse *nqo1* promoter reporter construct, containing the functional ARE (5′-TCACAGTGAGTCGGCAAAATT-3′) in the pGL3-Basic luciferase reporter vector, was described previously and was designated −1016/nqo5′-luc (29). The mutant NQO1 reporter construct containing 1016 nucleotides of 5′-upstream *nqo1* sequence but with the ARE scrambled (i.e., 5′-TTAGAGATACTAGACCACGTC-3′, with mutated bases in italics) is called Mut1 (29). Transfection of −1016/nqo5′-luc and Mut1 into Hepa-1c1c7 cells was performed using Lipofectin Reagent (Life Technologies), and, in all experiments, the pRL-TK *Renilla* reporter vector (Promega) was used as an internal control. Renilla and firefly luciferase activities were measured using the Dual-Luciferase Reporter Assay System (Promega).

RESULTS

Glucosinolates present in broccoli seeds

The glucosinolate content of broccoli seeds was examined before their ability to induce gene expression in mammalian cells was examined. Prior heating, to inactivate myrosinase, followed by LC-MS/MS analysis revealed that the seeds contained 38.8 mmol glucosinolates per kg. Glucoiberin accounted for 59% of the total glucosinolate recovered, whereas sinigrin and glucoraphanin accounted for 19 and 8% of the glucosinolates, respectively. Significant amounts of progoitrin, gluconapin, and gluconasturtiin were also detected (**Table 1**). The structures of these phytochemicals are shown in **Figure 1.**

Broccoli seeds induce NQO1 and GST in $nrf2^{+/+}$ *but not in* $nrf2^{-/-}$ *mice*

Feeding $nrf2^{+/+}$ mice diets containing 15% (w:w) crushed broccoli seeds resulted in the induction of both NQO1 and GST enzyme activities in the stomach, the small intestine, and the liver, but no increase was observed in the large intestine.

In the wild-type mice, feeding the seeds increased NQO1 activity in the stomach from 155 ± 40 to 248 ± 50 $nmol \cdot min^{-1} \cdot mg^{-1}$ protein; in the small intestine, the broccoli seed diet increased NQO1 activity from 106 ± 16 to 183 ± 8 $nmol \cdot min^{-1} \cdot mg^{-1}$ protein; and, in the liver, this diet increased NQO1 activity from 50 ± 7 to 72 ± 4 $nmol \cdot min^{-1} \cdot mg^{-1}$ protein. The NQO1 enzyme activity in the stomach, the small intestine, and the liver of $nrf2^{-/-}$ mice placed on a control diet was only 50 ± 16, 40 ± 20, and 7 ± 5 $nmol \cdot min^{-1} \cdot mg^{-1}$ protein, respectively. The NQO1 enzyme activity did not appear to be increased in stomach, the small intestine, or the liver of $nrf2^{-/-}$ mice fed diet containing broccoli seeds.

In $nrf2^{+/+}$ mice, feeding the broccoli seed diet for 7 d increased GST activity in the stomach from 1.55 ± 0.10 to 2.53 ± 0.47 $\mu mol \cdot min^{-1} \cdot mg^{-1}$ protein, in the small intestine from 1.61 ± 0.11 to 2.02 ± 0.23 $\mu mol \cdot min^{-1} \cdot mg^{-1}$ protein, and in the liver from 4.91 ± 0.52 to 7.7 ± 0.95 $\mu mol \cdot min^{-1} \cdot mg^{-1}$ protein. Not only was transferase activity substantially lower in $nrf2^{-/-}$ mice than in the wild-type mice, but also, it was not increased in the mutant mice fed broccoli seeds. In stomach, small intestine, and liver, GST activity in knockout mice on a control diet was 1.26 ± 0.11, 1.18 ± 0.12, and 1.72 ± 0.69 $\mu mol \cdot min^{-1} \cdot mg^{-1}$ protein, respectively.

The levels of NQO1 protein in the tissues of mice fed

TABLE 1

Glucosinolate content of broccoli seeds

Glucosinolate	Amount	%
	mmol/kg	
Sinigrin	7.5 ± 1.0	19
Gluconapin	1.3 ± 0.2	3
Progoitrin	2.7 ± 0.4	7
Glucoiberin	23.2 ± 3.6	59
Glucoraphanin	3.2 ± 0.4	8
Glucoalyssin	0.2 ± 0.04	1
Gluconasturtiin	0.9 ± 0.3	2

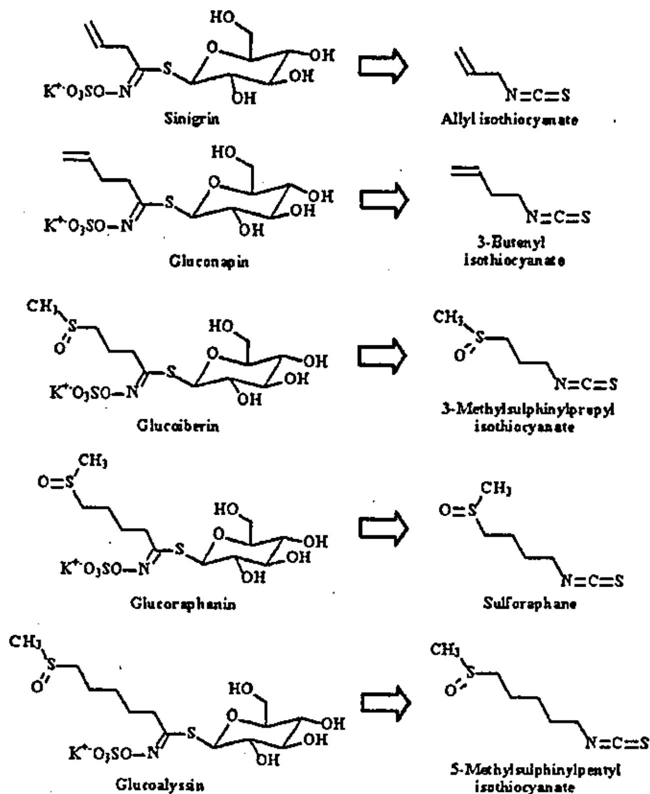

FIGURE 1 Glucosinolates (*left*) and ITCs (*right*) obtained from broccoli seeds.

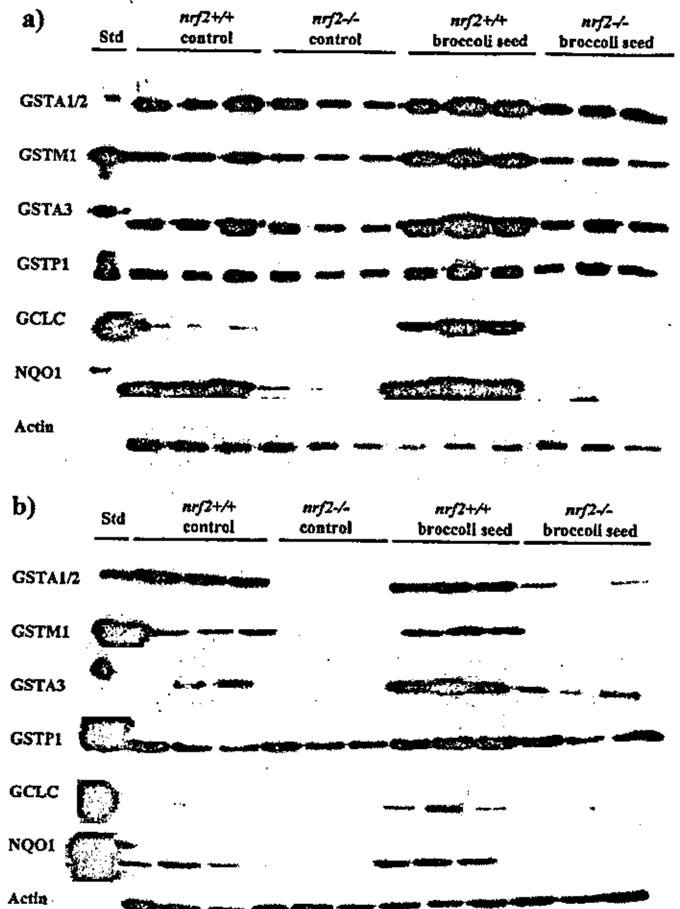

FIGURE 2 Nrf2-dependent induction of NQO1, GST, and GCLC proteins in stomach of mice fed broccoli seeds. Western blotting was performed on tissue extracts. Immunoreactive standards were applied to lane 1. Portions (10 μg protein) from stomach (*panel a*) or small intestine (*panel b*) of $nrf2^{+/+}$ and $nrf2^{-/-}$ mice fed on the RM1 control diet and from mice fed on RM1 diet containing 15% (w:w) crushed broccoli seeds were applied to the remaining lanes. Samples of tissue cytosol from 3 mice were applied to the gel.

broccoli seeds was examined by Western blotting to determine whether increases in oxidoreductase activity in stomach, small intestine, and liver reflected an increase in protein. Immunoblotting showed increases of ~2-fold in the level of NQO1 in all 3 organs from $nrf2^{+/+}$ mice administered broccoli seeds (Figs. 2 and 3). Similar experiments were carried out using antisera against class Alpha, Mu, and Pi GST subunits. These revealed significant increases of class Alpha GSTA3 protein in stomach and small intestine and a modest increase in all organs of class Mu GSTM1. The level of the class Pi GSTP1 subunit did not appear to increase in mice after administration of broccoli seeds.

Western blots showed a 5-fold increase in the level of GCLC in the stomach of $nrf2^{+/+}$ mice fed broccoli seeds, and a more modest increase was also observed in the small intestine of wild-type mice (Fig. 2). By contrast, no increase was observed in the liver (Fig. 3). A decrease in GCLC protein levels was seen in the stomach, the small intestine, and the liver of $nrf2^{-/-}$ mice compared with the same organs from wild-type mice. Furthermore, the protein was not induced in either stomach or small intestine of mutant mice fed broccoli seeds (Fig. 2).

Glucosinolate breakdown products identified in broccoli seed extracts

The total amount of glucosinolate in the broccoli seed extract was <3.6 μmol/L, whereas the total amount of ITC in the extract was 596 μmol/L. Table 2 shows that 3-methylsulfinylpropyl ITC and sulforaphane account for 61 and 30%,

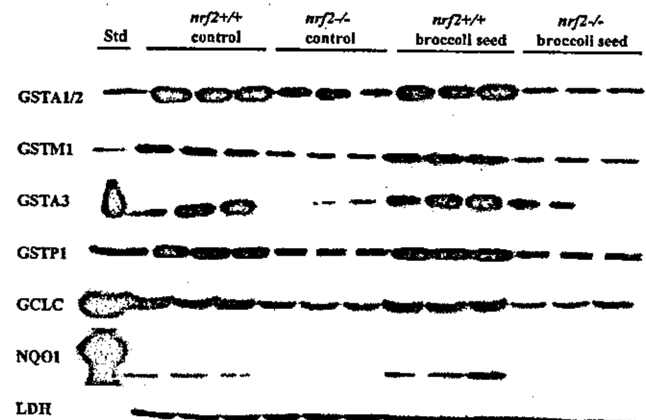

FIGURE 3 Induction of hepatic NQO1 and GST by broccoli seeds. Immunoblotting was performed on hepatic cytosol from wild-type and mutant mice as described. Lactate dehydrogenase (LDH) was used as a loading control for the samples.

TABLE 2

Isothiocyanates in broccoli seed extracts

Parent glucosinolate	Isothiocyanate	Amount of isothiocyanate[1]	
		µmol/L	%
Sinigrin	Allyl ITC	25.0	4.2
Gluconapin	3-Butenyl ITC	23.0	3.8
Progoitrin	5-Vinyloxazolidine-2-thione	nd	—
Glucoiberin	3-Methylsulfinylpropyl ITC	364.0	61.1
Glucoraphanin	Sulforaphane	177.0	30.0
Glucoalyssin	5-Methylsulfinylpentyl ITC	5.5	0.9
Gluconasturtiin	Phenethyl ITC	1.2	0.2

1 nd, not determined.

respectively, of the ITCs present in the seed extract. Significant amounts of AITC and 3-butenyl ITC were also obtained.

Induction of NQO1 and GST in rodent liver cell lines by broccoli-derived chemicals

Aqueous broccoli seed extracts were used to treat cells at an estimated concentration of total ITC of 0.6 µmol/L in the media. The transformed mouse Hepa-1c1c7 liver cell line and the nontransformed rat liver RL-34 epithelial cells were used in these experiments. The broccoli seed extract increased NQO1 enzyme activity ~3-fold and ~5-fold in the Hepa-1c1c7 and RL-34 cells, respectively. Treatment with AITC at 5 µmol/L induced NQO1 catalytic activity ~2-fold in both Hepa-1c1c7 and RL-34 cells. Treatment with sulforaphane at 5 µmol/L induced NQO1 catalytic activity 4.5-fold and 5.2-fold in Hepa-1c1c7 and RL-34 cells, respectively. By contrast, GST activity was not increased to the same extent in either cell line.

Western blotting showed that the level of NQO1 protein in Hepa-1c1c7 and RL-34 cells (Fig. 4A and B, respectively) grown in normal cell culture medium without the addition of phytochemicals was barely detectable. Treatment of both cell lines with the broccoli seed extract containing a mixture of ITCs substantially increased NQO1 protein. This increase was comparable to the induction of NQO1 protein affected by sulforaphane at 5 µmol/L.

Immunoblots were carried out to determine whether the broccoli extracts induced the various GST subunits. The levels of the class Alpha GSTA1/2 and GSTA3 subunits were found to be increased by the broccoli extract, and the degree of induction was similar to that obtained using sulforaphane.

In both Hepa-1c1c7 and RL-34 cells, the broccoli seed extract induced large increases in GCLC protein (Fig. 4).

Broccoli seed extracts stimulate ARE-driven gene expression

To determine whether broccoli seed extracts can activate gene expression controlled through an ARE enhancer, RL-34 cells were transfected with the mouse −1016/nqo5′-luc reporter construct. Treatment of transfected cells with the standard dose of broccoli seed extract produced a 4.6-fold increase in luciferase activity compared with transfected cells treated with vehicle alone (Fig. 5). By contrast, AITC and sulforaphane, each at 5 µmol/L, produced 1.9-fold and 3.3-fold

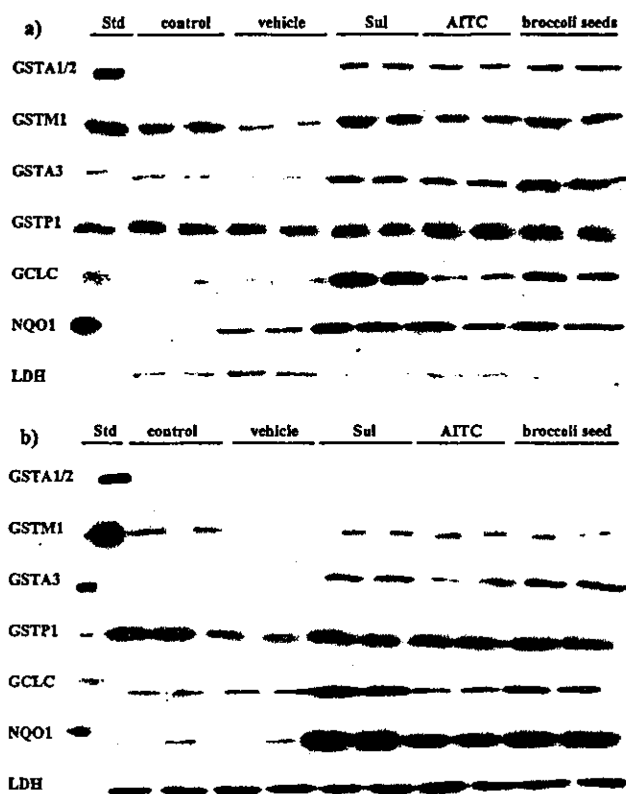

FIGURE 4 Induction of NQO1, GST, and GCLC by broccoli seed extracts in rodent liver cell lines. Cells were grown in either media alone or for 24 h in media containing sulforaphane (Sul; 5 µmol/L), AITC (5 µmol/L), or 1/1000 dilution of broccoli seed extract. Protein standards were applied to lane 1. The other samples are duplicates of individual treatments taken from separate flasks. Panel *A* shows data from the transformed Hepa-1c1c7 cells and panel *B* shows data from the nontransformed rat liver RL-34 cells.

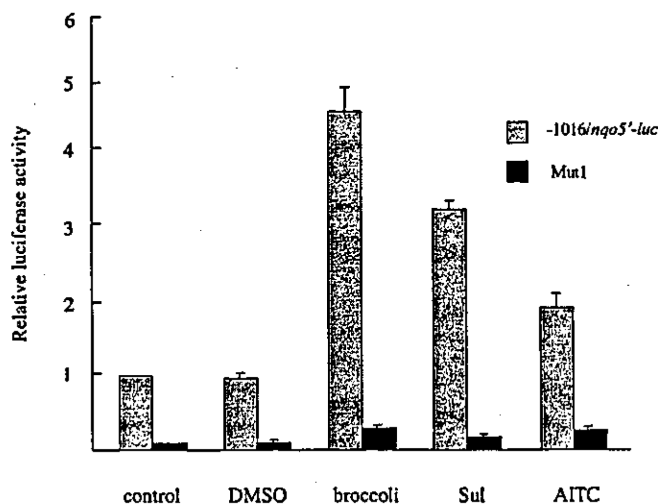

FIGURE 5 Broccoli seed extracts stimulate ARE–driven gene expression. Mouse Hepa-1c1c7 cells were transfected with a luciferase reporter construct driven by the wild-type mouse *nqo1* promoter (−1016/nqo5′-luc) or by the same promoter containing a scrambled ARE (Mut1); pRL-TK *Renilla* reporter vector was used as an internal control. Sixteen hours after transfection, cells were treated for 24 h with 1/1000 dilution of broccoli seed extract, sulforaphane (Sul; 5 µmol/L), AITC (5 µmol/L), or dimethyl sulfoxide (0.1% v:v).

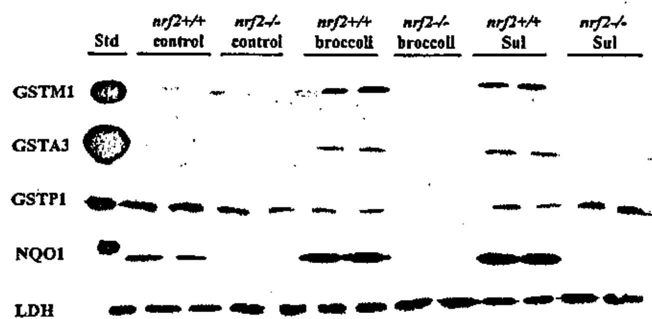

FIGURE 6 Nrf2-dependent induction of NQO1 and GST in mouse embryonic fibroblasts. Wild-type and Nrf2-null MEFs were derived and maintained as described. In the control treatment group the MEFs were grown in medium supplemented with epidermal growth factor, insulin-transferrin-selenium, and 10% fetal bovine serum. Treatment with broccoli seed extract involved growing MEFs in medium for 24 h with 1/1000 dilution of the filtered aqueous seed extract. The sulforaphane (Sul) treated MEFs were grown for 24 h in the presence of ITC (5 μmol/L).

increases, respectively, in luciferase activity. Similar experiments using a reporter construct driven by the mouse *nqo1* promoter that contained a mutant ARE (i.e., Mut1) proved to be unresponsive to broccoli seed extract, AITC, and sulforaphane.

Induction of GST and NQO1 by broccoli seed extracts is abolished in nrf2$^{-/-}$ mouse embryonic fibroblasts

To explore whether GST subunits and NQO1 can be induced by broccoli in an Nrf2-dependent fashion, wild-type and mutant MEFs were treated with the seed extract. In the *nrf2*$^{+/+}$ MEFs, treatment with the standard dose of broccoli seed extract caused a significant increase in GSTM1, GSTA3, and NQO1. This increase was similar to that seen in wild-type MEFs treated with sulforaphane at 5 μmol/L. In the *nrf2*$^{-/-}$ MEFs, the levels of GSTM1, GSTA3, and NQO1 were lower than in the wild-type cells, and the seed extract failed to induce these proteins (Fig. 6).

DISCUSSION

An increasing body of evidence suggests that high intake of cruciferous vegetables can protect against tumorigenesis (2–6). One mechanism proposed to explain this conclusion is that glucosinolates, which are uniquely abundant in these plants, are converted by the actions of myrosinase to thiol-active metabolites that can stimulate cytoprotective responses in cells of the host (40). The major group of phytochemicals that are believed to stimulate such defenses are ITCs, and these compounds can induce the expression of ARE-driven genes. An alternative hypothesis is that ITCs can cause arrest at the G2/M phase of the cell cycle. This is associated with decreases in cyclin B1, Cdc25B, and Cdc25C proteins (41).

Most of the studies into the cellular effects of glucosinolate-derived compounds have used purified phytochemicals such as sulforaphane, benzyl ITC, and phenethyl ITC (2,14–18). How relevant the doses of pure phytochemical used in such gene induction and cell cycle arrest experiments are to the in vivo situation is unclear. This issue is complicated, because the yield of ITCs from different parental glucosinolates varies substantially and can be influenced significantly by the presence of epithiospecifier protein present in certain crucifers (9,42). In the present paper, broccoli seeds were used as the source of plant glucosinolates because we wished to avoid variations in the content of these chemicals that arise from postgermination metabolism. Furthermore, Fahey et al. (43) reported that the ability of broccoli to induce NQO1 in Hepa-1c1c7 cells diminishes with the age of the plant. Therefore, in this study, we used crushed broccoli seeds in the mice feeding experiments and aqueous seed extracts in the cell culture experiments. Analysis of the glucosinolates revealed that the seeds used in this study contained primarily glucoiberin and sinigrin, with lesser amounts of glucoraphanin and progoitrin (Table 1). In the aqueous broccoli seed extracts, LC-MS/MS revealed the presence of large amounts of ITCs, primarily 3-methylsulfinylpropyl ITC, and sulforaphane (Table 2). The low recovery of AITC in the extracts is noteworthy given the large amount of sinigrin in the broccoli seeds.

Enzyme assay and Western blotting showed that addition of broccoli seeds at 15% (w:w) in the RM1 diet induced NQO1 about 2-fold in stomach, small intestine, and liver of wild-type mice. No induction was observed in the *nrf2*$^{-/-}$ mice. Similar results were observed by treating the *nrf2*$^{+/+}$ and *nrf2*$^{-/-}$ mouse embryonic fibroblasts with broccoli seed extracts. Because the promoter of mouse *nqo1* contains a functional ARE that recruits Nrf2 after treatment with sulforaphane (29), it is highly likely that transcriptional activation of mouse *nqo1* caused by preparations of broccoli seed is a direct consequence of ITCs stimulating the basic-region leucine zipper protein to transactivate directly the oxidoreductase gene.

Among GSTs, modest increases of GSTM1 protein were observed in the stomach and the small intestine of wild-type but not of *nrf2*$^{-/-}$ mice after feeding with broccoli seeds. This diet also produced significant increases of the GSTA3 subunit in the stomach and large increases in the small intestine of wild-type mice. However, no such increases were observed in mutant mice. In MEFs from the wild-type and knockout mice, the Nrf2 dependency of induction of GSTM1 and GSTA3 by broccoli was clearly observed. Both the GSTM1 and GSTA3 subunit genes have been reported to contain an ARE (30,44), and it is likely that Nrf2 mediates induction directly through this enhancer. Chromatin immunoprecipitation experiments are required to confirm this hypothesis.

In the stomach and the small intestine of wild-type mice, substantial increases in GCLC were observed after treatment with the broccoli seed preparations. It is likely that Nrf2 mediates the increase in mouse GCLC and requires the existence of a functional ARE in the gene promoter, because this occurs in the human gene (45). However, the presence of a functional ARE in mouse *gclc* remains to be established.

Cellular models for screening the cancer chemopreventive properties of phytochemicals have frequently used induction of NQO1 enzyme activity in Hepa-1c1c7 cells (46). Our study revealed that besides NQO1 induction, GSTA1/2, GSTA3, and GCLC are also increased significantly in this transformed cell line by broccoli seed extract and by sulforaphane. Importantly, we also found that in nontransformed RL-34 cells, the seed extract and sulforaphane cause large increases in NQO1 and GCLC proteins. Modest increases in GSTA3 were also observed. Nakamura et al. (13) suggested that measurement of GST activity in RL-34 cells provides a useful assay for identifying potential inducing agents. However, our data suggest that induction of NQO1 in these cells may provide the most